

Diblock Copolymer Micelles in a Dilute Solution

Ekaterina B. Zhulina,^{†,‡} Mireile Adam,[†] Isaac LaRue,[†] Sergei S. Sheiko,[†] and Michael Rubinstein^{*,†}*Department of Chemistry, University of North Carolina, Chapel Hill, North Carolina 27599-3290, and Institute of Macromolecular Compounds, Russian Academy of Sciences, St. Petersburg 199004, Russia**Received September 14, 2004; Revised Manuscript Received March 25, 2005*

ABSTRACT: We performed theoretical and experimental investigations of dilute solutions of micelles of neutral amorphous diblock copolymers in selective solvents. The ranges of thermodynamic stability of spherical, cylindrical, and lamellar morphologies along with the equilibrium sizes and aggregation numbers of micelles are calculated and measured. For high molecular weight copolymers it is shown that the sphere-to-cylinder transition as well as precipitation of the micelles associated with cylinder-to-lamella transition occurs when aggregates have a crew-cut structure with the thickness of the corona smaller than the radius of the core. Similar to starlike micelles with corona larger than the core, the equilibrium parameters of crew-cut micelles are determined by the balance between the free energy of the corona and the surface energy of the core. The elastic free energy of the core remains small compared to the corona and surface free energies; however, it determines the transitions between different morphologies. The theoretical predictions including the existence of crew-cut spherical micelles, the range of stability of cylindrical micelles, and the significance of the contributions of the logarithmic corrections to scaling are in good agreement with experiments on polystyrene–polyisoprene block copolymer micelles in heptane, a selective solvent for the polyisoprene block.

1. Introduction

Diblock copolymers in selective solvents self-assemble into aggregates of various morphologies. The insoluble component associates to form a denser core of the aggregate, whereas the soluble component organizes into a corona that prevents the aggregates from precipitating. For copolymers with flexible blocks, the morphology of the aggregates depends on the chemical composition of the molecules. When the soluble block is long, spherical micelles are found in dilute solutions. A decrease in the length of the soluble block leads to a change in micelle morphology and eventual precipitation of the aggregates from the solution. The general features of spherical micelles in dilute solutions were investigated both theoretically and experimentally. Development of the scaling concepts^{1,2} and application of these ideas to micellization phenomena provided the power law dependences for the equilibrium parameters of spherical aggregates.^{3–7} A number of experimental studies confirmed the general features of the theoretical predictions for properties of spherical micelles (see, for example, ref 8 and references therein). However, the experimentally measured values of the corresponding exponents often deviate from the theoretical predictions.⁹ The discrepancies are usually attributed to slow kinetics and lack of system equilibration, sample impurities, and molecular weight polydispersity.

The situation with micelles of nonspherical morphologies (cylinders, bilayers, etc.) is even more complicated. The experimental observations of cylindrical micelles in dilute solutions are still rather limited. The existence of long cylindrical aggregates was demonstrated for copolymers with a water-soluble corona block such as polybutadiene–poly(ethylene oxide) (PB–PEO)¹⁰ and polystyrene–poly(acrylic acid) (PS–PAA).¹¹ Cylindrical micelles were also observed in organic solvents. Experi-

mental studies on polystyrene–polyisoprene (PS–PI) block copolymers in organic solvents indicated the presence of long cylindrical micelles with PS core and PI corona^{12–15} as well as micelles with PI core and PS corona.^{16,17} However, the question of whether the observed aggregates were equilibrium structures still remains open. In a recent small-angle neutron scattering (SANS) study¹⁸ of PB–PEO giant cylindrical micelles, no detectable exchange of unimers between aggregates and solution was observed. This freezing of the core and prohibition of any micelle rearrangements were attributed to extremely high hydrophobicity of the PB block. The slow equilibration as well as the narrow stability range makes experimental studies of cylindrical micelles at equilibrium very challenging. The experimental studies of the stability range for different micellar morphologies are also hindered by the lack of quantitative theoretical predictions^{4–7} and computer simulations¹⁹ in the experimentally relevant range of parameters.

In previous theoretical studies, the scaling model was used to delineate the scaling laws for parameters of equilibrium micelles.^{4–7} This was done by balancing the two dominant contributions to the free energy of the micelle (elastic energy of the corona and the surface energy of the core), whereas the third contribution (elastic energy of the core) and all the numerical coefficients were omitted. If the micellar corona is much larger than the core (hairy micelle regime), the micelles of different morphologies exhibit different scaling laws. This is because the structure of the corona (wet polymer brush) is sensitive to the space dimension and therefore has different polymer density profiles in lamellar, cylindrical, and spherical coronas. For the corona much smaller than the core (crew-cut micelle regime), all three ingredients in the free energy scale in a similar way for micelles of different morphologies. As a result, they exhibit the same scaling laws.

[†] University of North Carolina.

[‡] Russian Academy of Sciences.

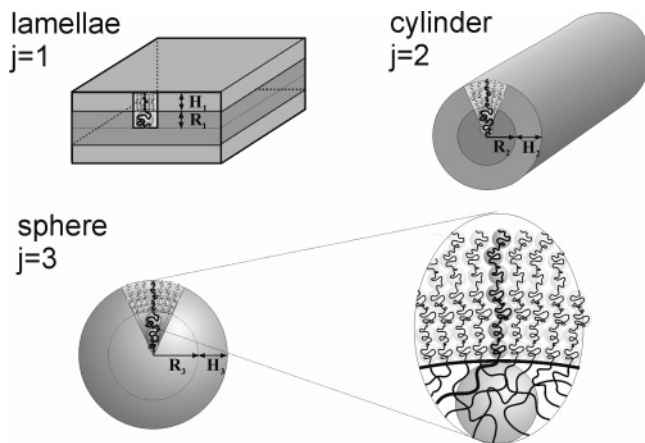


Figure 1. The scaling model is used to explain configuration of chains in the core and in the corona of diblock copolymer micelles of different geometries: lamellar, cylindrical, and spherical micelles. One can consider a chain in the corona as a string of correlation blobs. Since the core block experiences net attraction, one can consider the core as a system of much larger tension blobs. The corona contains more blobs per chain than the core, and the corona free energy dominates over elastic stretching of the core blocks.

In contrast to these studies, we retain the full expressions for the free energy as a function of the core radius as well as all the numerical coefficients. This allows us to develop a quantitative theory for equilibrium structures of aggregates that are formed in dilute solutions of neutral diblock copolymers in selective solvents. We focus on micelles of three major morphologies (spheres, cylinders, and lamellae), calculate their equilibrium parameters (aggregation number, core and corona sizes, etc.), and explore their ranges of stability. Although our variables are determined only up to numerical prefactors, they still indicate how variations in the lengths of the blocks affect the stability range of cylindrical micelles.

The schematics of the micellar morphologies are shown in Figure 1. We will demonstrate that for long chains both the sphere–cylinder and cylinder–lamellae transitions occur in the so-called crew-cut regime where the thickness of the swollen corona is smaller than the radius of the dense core. We emphasize that despite the small size of the corona, its free energy can still be significantly larger than the elastic energy of the core. This is because the corona chains are more extended with respect to their unperturbed size than the insoluble core blocks (which results in large entropic costs). Similar to wet planar brushes,^{20–22} excluded volume (for good solvent) and three-body (for Θ solvent) repulsions between monomeric units in the corona cause strong extension of the densely tethered chains. One can consider a chain in the corona as a string of correlation blobs that do not overlap² [there is some overlap of correlation blobs in the lateral direction in a Θ solvent in the case of the Kuhn segment larger than the monomer size (see Appendix I)]. On the contrary, the core chains experience net attraction between the monomeric units and therefore do not need to be strongly extended to fill the core. One can consider the core as a system of overlapping tension blobs with size much larger than the size of the corona blobs. As shown in Figure 1, the corona contains more blobs per chain than the core, and therefore, the corona free energy dominates over the elastic stretching of the core blocks. Note that the chain free energy is proportional to the number of blobs per chain.^{1,2}

Extension of chains both in the corona and in the core depends on the area per chain which is determined by the balance of the elastic energy of the corona and the surface energy of the core. Note that the corona always prefers a spherical geometry; however, this preference weakens with decreasing the length of the corona chains. Therefore, the transitions between different morphologies are driven by the core chains that prefer cylindrical or lamellar morphologies since they allow lower extensions of the core blocks. In other words, if a spherical micelle becomes cylindrical, this leads to an increase in free energy of the corona block and to a decrease in free energy of the core block. This balance becomes favorable toward cylindrical morphologies in the crew-cut regime, wherein decreasing the length of the corona block leads to the decrease of the total number of corona blobs and thus the blob penalty due to the sphere–cylinder transition. Here it is important to note that the thin corona in crew-cut micelles can be treated as an almost planar brush and therefore the elastic energy depends only weakly on the morphology type. Below we will show that the change in the corona free energy results from correction terms in the free energy of a planar brush due to the small curvature, whereas the changes in the core free energy result from the main term. This aspect is illustrated in Figure 1, where the change in the number of corona and core blobs is relatively small compared to the total number of blobs in a corona block; however, it is significant in comparison with to the total number of blobs in a core block.

We compare theoretical predictions with experimental data on PS–PI diblock copolymers in heptane. The theoretical parameters are first adjusted to fit the experimental data on spherical micelles. Then using these fixed parameters, the theoretical predictions are obtained for cylindrical micelles (their structure and stability range) and are compared with experimental data. A good agreement between the theory and experiment is established. We delineate the phase diagram of the block copolymer solution and determine the boundaries between micelles of different morphologies.

2. Model

We consider flexible diblock copolymers that contain $N_A \gg 1$ and $N_B \gg 1$ monomers with respective sizes a_A and a_B . The selective solvent is assumed to be good or Θ for block A and poor for block B. When the concentration of polymer in solution is above the so-called critical micelle concentration (cmc), micelles of various morphologies form (see Figure 1). Blocks B associate to form the core of the micelle, whereas blocks A form the corona which ensures solubility of aggregates in solution. We consider the aggregates of three different morphologies labeled by index j : lamellar ($j = 1$), cylindrical ($j = 2$), and spherical ($j = 3$). We also consider unimers (i.e., isolated diblocks) identified by $j = 0$ (see Figure 1).

To examine the equilibrium structure and thermodynamic stability of micelles, we focus on their free energy, F_j . Below we separately consider three main components of this free energy

$$F_j = F_{Bj} + F_{sj} + F_{Aj} \quad (1)$$

where F_{Bj} , F_{sj} , and F_{Aj} are the free energies per chain of the micellar core, of its surface, and of the corona.

2.1. Free Energy of the Core. The micellar core is partially swollen by poor solvent. We assume that the

volume fraction φ of monomers B in the micellar core is independent of the shape of the micelle and distance r from its center. For a core with low polymer density, $\varphi \ll 1$, the equilibrium volume fraction is determined by the balance of the attractive pair and repulsive ternary contacts between monomers, $\varphi \sim \tau$, where τ is the relative deviation from the θ -temperature, $\tau = (T - \theta)/T$, for polymer B . For larger values of the volume fraction φ , the higher-order monomer–monomer interactions are relevant. The free energy of the monomer–monomer interaction per block B is independent of the total number of chains in the micelle and coincides with the free energy F_{B0} in the collapsed core of a unimer (isolated diblock in solution). We can therefore omit it from further consideration because it does not contribute to the free energy difference between unimer and micelles of different morphology and aggregation number. If R_j is the radius of the core and s is surface area per chain, then the volume fraction of polymer in the core φ is

$$\varphi = \frac{jN_B \alpha_B^3}{sR_j} \quad (2)$$

where $j = 1, 2$, and 3 corresponds to lamellar, cylindrical, and spherical core. From eq 2 we find the radius of the core (in lamella, R_1 is half of core thickness)

$$R_j = \frac{jN_B \alpha_B^3}{\varphi s} \quad (3)$$

and the surface area per chain

$$s = \frac{jN_B \alpha_B^3}{\varphi R_j} \quad (4)$$

Here and below we denote generalized (unrestricted) values of the surface area per chain by s while the equilibrium surface area per chain in a micelle with morphology j is denoted by s_j . For micelles with large aggregation number, blocks B are stretched in the core⁴ with respect to their Gaussian end-to-end distance

$$R_G = \sqrt{a_B N_B l_B} = a_B \sqrt{p_B N_B} \quad (5)$$

where

$$p_B = l_B / a_B$$

is the ratio of the Kuhn segment l_B and monomer size a_B . The elastic free energy F_{Bj} of blocks B in the core of morphology j is described as

$$\frac{F_{Bj}}{kT} = k_j \frac{R_j^2}{R_G^2} = k_j \frac{R_j^2}{a_B^2 N_B p_B} = k_j^2 \frac{\alpha_B^4 N_B}{p_B s^2 \varphi^2} \quad (6)$$

We approximate the elastic free energy of blocks B by eq 6 in the whole range of chain stretching $R_j/R_G \gtrsim 1$ (ignoring nonlinear elongation). The numerical coefficients k_j were calculated by Semenov²³ and are given by

$$k_1 = \pi^2/8, \quad k_2 = \pi^2/16, \quad k_3 = 3\pi^2/80 \quad (7)$$

Note that the values of k_j given by eq 7 were obtained for the specific case of a dense core ($\varphi = 1$). They,

however, remain valid for an arbitrary volume fraction φ of monomers B provided that the polymer density profile in the core is uniform. As discussed in the Introduction and derived below, the elastic contribution F_{Bj} remains small compared to the surface and corona free energies in stable micelles. However, it becomes important in determining the transitions between different morphologies.

2.2. Surface Free Energy. The surface free energy per chain F_{sj} for morphology j is associated with the interface between the core and the corona. This energy is proportional to the surface area per chain s (eq 4)

$$\frac{F_{sj}}{kT} = \tilde{\gamma} s = \gamma (s/\alpha_B^2) = \gamma \frac{jN_B \alpha_B}{\varphi R_j} \quad (8)$$

where $\tilde{\gamma}$ is the surface free energy per unit area (surface tension) and $\gamma = \tilde{\gamma} \alpha_B^2$ is the surface free energy per area α_B^2 , both divided by kT . At low polymer volume fractions in the core ($\varphi \ll 1$) there is a scaling relation between the surface tension $\tilde{\gamma}$ and the volume fraction φ ($\tilde{\gamma} \sim \varphi^2$).^{1,2} However, we focus below on relatively high values of the polymer volume fraction in the core, $\varphi \lesssim 1$, which is relevant to most experiments. In this range of polymer concentrations the conventional scaling model^{1,2} may not work, and in the following we use γ as an additional independent parameter of the model.

The expression for the surface free energy per chain F_{sj} (eq 8) is valid for any morphology j . For example, for an isolated spherical globule ($j = 0$) of a single collapsed block B , the radius of the core is

$$R_{B0} = \alpha_B \left(\frac{3N_B}{4\pi\varphi} \right)^{1/3} \quad (9)$$

and the surface free energy of a unimer yields

$$\frac{F_{s0}}{kT} = 4\pi\tilde{\gamma}R_{B0}^2 = 4\pi\gamma \left(\frac{R_{B0}}{\alpha_B} \right)^2 = 4\pi\gamma \left(\frac{3N_B}{4\pi\varphi} \right)^{2/3} = (36\pi)^{1/3} \gamma \left(\frac{N_B}{\varphi} \right)^{2/3} \quad (10)$$

In section 5.1 we will use eq 10 to estimate γ from the scattering data reported in ref 24.

2.3. Free Energy of the Corona. Because of the narrow interface between blocks A and B , the corona blocks A can be envisioned as tethered to the surface of the micellar core. The equilibrium structure of the corona is determined by the balance of the elastic stretching of blocks A and the repulsive interaction between monomers (two-body in a good solvent and three-body in a Θ solvent). We apply scaling analysis^{1,2} to calculate the free energy of the corona chains, assuming that the free ends of the corona chains are localized at the outer boundary of the micelle. Within the framework of the scaling theory of polymer brushes, the corona of the micelle in a good solvent is envisioned as a melt of correlation blobs of size ξ_A (sections of chains interacting with each other with energy kT). A similar picture can be also applied to flexible chains in a Θ solvent. However, for stiffer chains in a Θ solvent with Kuhn segments larger than monomer size, correlation blobs overlap in the lateral direction (see Appendix I). These correlation blobs have the same size in lamellar aggregates, while they increase in size from the core to the periphery in the corona for spherical and cylindrical micelles.^{20,22,25,26,27}

The thermodynamic quality of the solvent for corona block A is governed by the magnitude of the monomeric excluded volume $\nu a_A^3 > 0$. We assume that the values of the dimensionless excluded-volume parameter ν and of the stiffness parameter

$$p_A = l_A/a_A > 1 \quad (11)$$

are insufficient to ensure swelling of the blobs in the corona of micelle. If the size of the largest blob ξ_A is smaller than size of the thermal blob, $\xi_t \approx p_A^2 \nu^{-1} a_A$ (i.e., $\xi_A < \xi_t$),^{1,2} a blob consisting of g_A monomers obeys the Gaussian statistics

$$\xi_A \approx a_A p_A^{1/2} g_A^{1/2} \quad (12)$$

which is valid in coronas of all morphologies.⁴ When the smallest blob size $\xi_A > \xi_t$, all the blobs in the corona are swollen, and the brush is found under good solvent conditions. Both cases are considered in Appendix I, wherein we present a systematic derivation for the structural properties of polymer brushes. In the main text, we will model the corona of respective micelle as a planar ($j = 1$), cylindrical ($j = 2$), or spherical ($j = 3$) brush in a Θ solvent with blob size ξ_A given by eq 12.

One may also consider a third possibility of thermal blob size ξ_t being intermediate between the smallest and the largest correlation blob sizes. In this case, smaller correlation blobs closer to the core of cylindrical or spherical micelle (with $\xi_A < \xi_t$) are Θ -like, while chain sections inside larger correlation blobs in the outer part of the corona (with $\xi_A > \xi_t$) are partially swollen. We will not consider this intermediate case in the present paper.

3. Properties of Micelles

Equilibrium properties of micelles are obtained by minimization of the total free energy per chain F_j (eq 1), including specific contributions defined in sections 2.1–2.3. Here we introduce the dimensionless radius of the core $r_j = R_j/a_B$ as an independent parameter. Minimization of micelle free energy per chain F_j with respect to the dimensionless core radius r_j is equivalent to minimization of free energy F_j with respect to the micelle aggregation number (that is, the number of chains in a spherical micelle, the number of chains per unit length in a cylindrical micelle or per unit area in a lamella).

3.1. Spherical Micelle. In the main part of the paper we focus on micelles in a Θ solvent, while in Appendices I–III we consider both the cases of good and Θ solvents. Taking into account eqs 1, 4, 6, 8, AI.1a, AI.2a, and AI.29 for $\nu = 1/2$, we represent the free energy of a block copolymer chain in a spherical micelle as

$$\frac{F_3}{kT} = \frac{3\pi^2 r_3^2}{80 p_B N_B} + \gamma \frac{3N_B}{\varphi r_3^2} + \frac{1}{2\sqrt{3}} C_{FP_A}^{-3/4} \frac{r_3^{3/2} \varphi^{1/2}}{N_B^{1/2}} \ln \left[1 + \frac{2C_H p_A^{1/4} N_A \varphi^{1/2} a_A^2}{\sqrt{3} r_3^{1/2} N_B^{1/2} a_B^2} \right] \quad (13)$$

where C_F and C_H are numerical coefficients on the order of unity. By minimizing free energy per chain F_3 with respect to dimensionless radius of the core $r_3 = R_3/a_B$ ($\delta F_3/\delta r_3 = 0$), we arrive at a nonlinear equation that determines the equilibrium value of r_3

$$\frac{3\pi^2 r_3}{40 p_B N_B} - \gamma \frac{3N_B}{\varphi r_3^2} + \frac{\sqrt{3}}{4} C_{FP_A}^{-3/4} \frac{r_3^{1/2} \varphi^{1/2}}{N_B^{1/2}} \ln \left[1 + \frac{2C_H p_A^{1/4} N_A \varphi^{1/2} a_A^2}{\sqrt{3} r_3^{1/2} N_B^{1/2} a_B^2} \right] - \frac{1}{6} \left(\frac{a_A}{a_B} \right)^2 \frac{C_F C_H N_A p_A^{-1/2} \varphi}{N_B \left[1 + \frac{2C_H p_A^{1/4} N_A \varphi^{1/2} a_A^2}{\sqrt{3} r_3^{1/2} N_B^{1/2} a_B^2} \right]} = 0 \quad (14)$$

This nonlinear equation for dimensionless core radius r_3 can be solved numerically. By substituting the numerical solution r_3 of eq 14 into eq 13, we find the free energy F_3 per molecule in an equilibrium spherical micelle.

From the dimensionless core radius r_3 (solution of eq 14), one also finds the corona thickness H_3 (Appendix AI). By substituting $\nu = 1/2$ in eq AI.30 and using eq AI.1a, we obtain the thickness of the corona

$$H_3 = R_3 \left[\left(1 + \frac{2C_H p_A^{1/4} N_A \varphi^{1/2} a_A^2}{\sqrt{3} r_3^{1/2} N_B^{1/2} a_B^2} \right)^{1/2} - 1 \right] \quad (15)$$

and the total size of a spherical micelle

$$R_3^{\text{tot}} = R_3 + H_3 \quad (16)$$

Aggregation number (total number of chains per micelle) Q is given by

$$Q = \frac{4\pi r_3^3 \varphi}{3N_B} \quad (17)$$

Lines 3 in Figure 2a,b demonstrate the dimensionless core radius R_3/a_B and corona thickness H_3/a_A in a spherical micelle as a function of N_A (degree of polymerization of corona block) calculated from eqs 14 and 15. Figure 2a,b also includes the corresponding curves for cylindrical and lamellar aggregates. The set of model parameters is specified in the figure legend and is the same in all subsequent figures. The thick solid lines correspond to equilibrium regimes of different morphologies. The thin vertical lines at N_A^{sc} and N_A^{cl} are the locations of the sphere-to-cylinder and the cylinder-to-lamella transitions, respectively. The details of these transitions will be explained in section 4. Figure 2a,b also includes asymptotic lines that can be calculated analytically as demonstrated in subsequent sections.

3.1.1. Asymptotic Dependencies of Spherical Micelles. Equations 13–17 determine the equilibrium characteristics for spherical micelles at different values of N_A and N_B . However, these equations are rather complicated and can be solved only numerically. Therefore, frequently one uses asymptotic expressions obtained for either very long or very short corona blocks. In this section, we summarize the asymptotic expressions for aggregation number and size of starlike ($H_3 \gg R_3$) and crew-cut ($H_3 \ll R_3$) micelles by delineating the leading terms in the free energy per chain F_3 .

Starlike Spherical Micelle ($H_3 \gg R_3$). In section 4 we demonstrate that for a starlike micelle the stretching

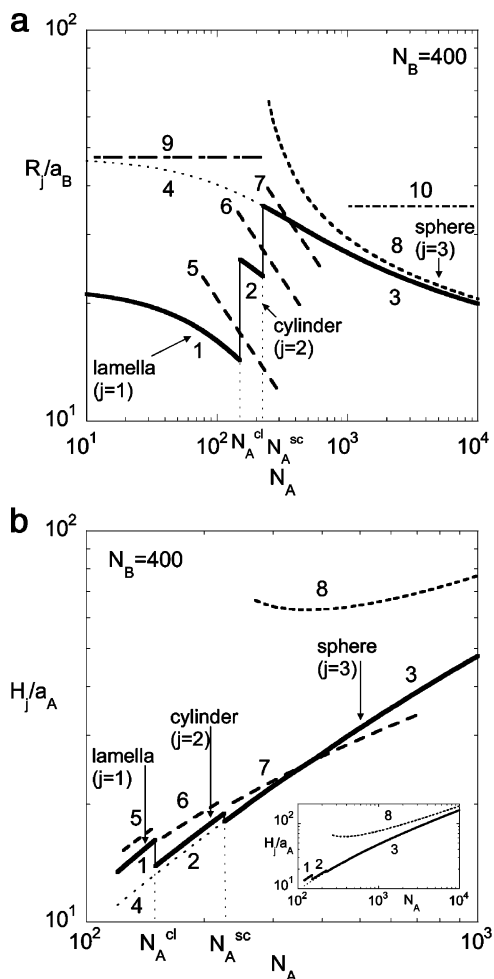


Figure 2. (a) Plot of the dimensionless radius of the micelle core R_j/a_B as a function of the degree of polymerization of the soluble block N_A . The plot shows both exact solutions and asymptotic values. Thick solid curves are exact solutions (eq 3) for lamella (1), cylinders (2), and spheres (3). The thin solid lines denote the transition from one morphology to another. The dotted line (4) denotes the size spherical micelles would adopt if they did not change morphology. The dashed lines are crew-cut asymptotes for lamella (5), cylinders (6), and spheres (7) from eqs 42, 36, and 25, respectively. The short-dashed line (8) is the starlike spherical asymptote (eq 18). The long dashed-short dashed line (9) denotes the asymptotic dependence for crew-cut spherical micelles for small values of N_A . While curve (4) approaches the asymptotic line (9) for small N_A , at this point the micelles have changed morphology, and therefore the asymptote (9) is not particularly relevant. The dotted-dashed line (10) denotes the variation in the core radius of starlike spherical micelles when the logarithmic term is ignored; i.e., K is set equal to unity. (b) Plot of the dimensionless thickness of the micelle corona H_j/a_A as a function of the degree of polymerization of the soluble block N_A . The plot shows both exact solutions and asymptote values. Thick solid curves are exact solutions of eqs 40, 32, and 15 for lamella (1), cylinders (2), and spheres (3), respectively. The thin solid lines denote the transition from one morphology to another. The dotted line (4) denotes the size spherical micelles would adopt if they did not change morphology. The dashed lines are crew cut asymptotes for lamella (5), cylinders (6), and spheres (7). The short-dashed line (8) is the asymptotic dependence for starlike spherical micelles (eq 21). The inset demonstrates that the starlike asymptote (8) for $N_B = 400$ approaches the numerical solution only as N_A becomes on the order of 10^4 . Here and in subsequent figures model parameters are $a_B = 5.6$ Å, $a_A = 5.0$ Å, $p_B = 1.5$, $p_A = 1.6$, $\varphi = 0.7$, $\gamma/\varphi^{2/3} = 0.097$, $C_F = 1.38$, and $C_H = 0.68$.

free energy F_{B3} of core block B can be neglected. The structure of the micelle is determined by the balance of the corona and surface free energies. By substituting $\nu = 1/2$ in eq AII.2 and using eqs AI.1a and AI.2a, we arrive at the scaling expression⁴ for the core radius of a starlike micelle

$$R_{3\text{star}} \approx a_B \left(\frac{N_B}{\varphi} \right)^{3/5} \left(\frac{4\sqrt{3}p_A^{3/4}}{C_F K} \gamma \right)^{2/5} \sim a_B \left(\frac{N_B}{\varphi} \right)^{3/5} \left(\frac{\gamma}{K} \right)^{2/5} \quad (18)$$

where the logarithmic term is denoted by (see eqs AII.3 and AI.1a)

$$K = \ln \left(\frac{2C_H p_A^{1/4} a_A^2 N_A \varphi^{1/2}}{\sqrt{3} a_B^2 N_B^{1/2} r_{3\text{star}0}^{1/2}} \right) \quad (19)$$

and from eqs AII.4 and AI.2a

$$r_{3\text{star}0} = \left(\frac{N_B}{\varphi} \right)^{3/5} \left(\frac{4\sqrt{3}p_A^{3/4}}{C_F} \gamma \right)^{2/5} \quad (20)$$

Here, $r_{3\text{star}0}$ is the dimensionless core radius if the logarithmic dependence of the corona free energy is totally neglected, and K is treated as a constant equal to unity. This leads to the incorrect conclusion that the core radius does not depend on the length of the corona block N_A (see dotted-dashed line 10 in Figure 2a). In contrast to ref 4, we retain here the numerical coefficients in order to proceed below with the analysis of experimental data. The short-dashed line 8 in Figure 2a shows the asymptotic behavior of the core radius $R_{3\text{star}}$ for starlike spherical micelles (eq 18). For $N_B = 400$ this curve is within 10% of the exact numerical solution of eq 14 for the values of the degree of polymerization of the corona block, N_A , larger than 3000.

The thickness of the corona $H_{3\text{star}}$ in a starlike micelle is obtained from eqs AII.5 ($\nu = 1/2$), AI.1a, and AI.2a

$$H_{3\text{star}} \approx a_A N_A^{1/2} \left(\frac{4\sqrt{3}}{C_F K} \gamma \right)^{3/10} \left(\frac{N_B}{\varphi} \right)^{1/5} p_A^{7/20} \left(\frac{2C_H}{\sqrt{3}} \right)^{1/2} \quad (21)$$

The short-dashed line 8 in Figure 2b shows the asymptotic behavior of the corona thickness $H_{3\text{star}}$ for starlike spherical micelles (eq 21). For $N_B = 400$ this curve is within 10% of the exact numerical solution of eq 15 for the values of N_A on the order of 10^4 (see inset).

From the core radius (eq 18) one can also determine the aggregation number $Q_{3\text{star}}$ (eq 17) of a starlike micelle as

$$Q_{3\text{star}} = \frac{4\pi\varphi r_{3\text{star}}^3}{3N_B} \approx \frac{4\pi}{3} \left(\frac{4\sqrt{3}p_A^{3/4}}{C_F} \frac{\gamma}{K} \right)^{6/5} \left(\frac{N_B}{\varphi} \right)^{4/5} \quad (22)$$

Figure 3 summarizes the predictions of the aggregation number Q as a function of the degree of polymerization of the corona block N_A , including the different asymptotes and the numerical solution. The solid line in Figure 3 is the plot of the aggregation number Q of the spherical micelle calculated according to eqs 14 and 17. The short dashed line indicates the starlike asymptote $Q_{3\text{star}}$ determined by eq 22. The dash-dotted line obtained from eqs 20 and 17 corresponds to the asymptote that does not account for the logarithmic dependence on N_A (by setting $K = 1$). Figure 3 demonstrates that in the range of $N_A \gtrsim 10^3$ and $N_B \approx 400$ the starlike

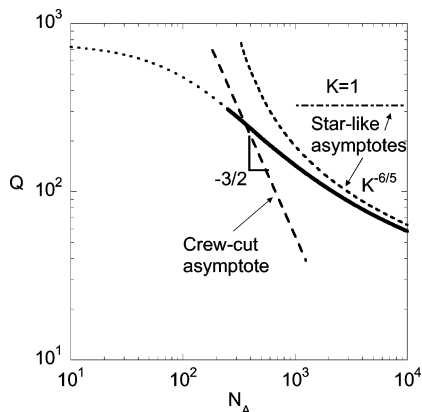


Figure 3. Aggregation number Q (eq 17) of a spherical micelle as a function of the degree of polymerization of the corona block N_A . The solid line is the analytical solution (eq 17). The dotted line is the aggregation number the micelles would have if they did not change morphology. Asymptotic dependences for crew-cut (eq 27) and starlike (eq 22) micelles are shown by long and short dashed lines, respectively. The dashed-dotted line is an asymptote for starlike micelles when eq 20 is used instead of eq 18, i.e., when the logarithmic term is equal to unity, $K = 1$, for all values of N_A . The set of model parameters is the same as in Figure 2.

asymptote without the logarithmic correction (dash-dotted line) overestimates the aggregation number Q by almost an order of magnitude. The starlike asymptote with logarithmic term (short dashed line) approaches the numerical solution for $N_A > 10^3$.

The asymptotic expression for the free energy per chain of starlike micelle (eqs AII.7 and AI.2a) yields

$$F_{3\text{star}}/kT \approx 5\gamma^{3/5} \left(\frac{C_F p_A^{-3/4} K N_B}{4\sqrt{3}\varphi} \right)^{2/5} \quad (23)$$

Expressions 18–23 indicate that all equilibrium parameters of starlike micelles (except for the corona thickness H_3) depend only logarithmically on the molecular weight of the corona block N_A (see short dashed line in Figure 3). Scaling analysis often ignores logarithmic terms and treats them as constants by setting $K = 1$ (see for example dashed–dotted lines in Figures 2a and 3). However, as will be shown below, this weak logarithmic dependence turns out to be essential to rationalize the experimental data.

Crew-Cut Spherical Micelle ($H_3 \ll R_3$). Micelles with the thickness of the corona smaller than the radius of the core are called crew-cut micelles. We emphasize that the definition of the crew-cut morphology is based on the geometric dimensions rather than on the ratio of the molecular weights of the blocks or on their contributions to the free energy of the micelle. Thus, by equating $H_{3\text{star}} = R_{3\text{star}}$ (eqs 18 and 21), we find the scaling boundary between the two morphologies.⁴

$$N_B^*(N_A) \approx \left(\frac{2}{3}\right)^{3/4} C_H^{5/4} N_A^{5/4} \varphi \left(\frac{C_F K}{\gamma}\right)^{1/4} p_A^{1/8} \left(\frac{\alpha_A}{\alpha_B}\right)^{5/2} \quad (24)$$

Here $N_B^*(N_A)$ is the degree of polymerization of the B block at which the size of the core is equal to the size of the corona for a given value of N_A . For a crew-cut micelle (i.e., when $N_B \gg N_B^*$), eqs AII.12, AI.1a, and AI.2a give

$$R_{3\text{cc}} \approx \frac{3N_B}{\varphi} \frac{\alpha_B^2}{\alpha_A} \left(\frac{\gamma p_A^{1/2}}{C_F C_H N_A} \right)^{1/2} \quad (25)$$

This asymptotic dependence is depicted by line 7 in Figure 2a. While the absolute values are close to the numerical solution of eq 14, their functional dependence is quite different. The area per chain (eq 4) in a crew-cut micelle (eqs AII.9, AI.1a, and AI.2a)

$$s_{\text{cc}} = \alpha_A \alpha_B \left(\frac{C_F C_H N_A}{\gamma p_A^{1/2}} \right)^{1/2} \quad (26)$$

increases as $s_{\text{cc}} \sim N_A^{1/2}$ whereas the aggregation number defined in eq 17 is (eqs AII.14, AI.1a, and AI.2a)

$$Q_{\text{cc}} = \frac{4\pi r_3^3 \varphi}{3N_B} \approx \frac{36\pi N_B^2}{\varphi^2} \left(\frac{\gamma \alpha_B^2 p_A^{1/2}}{C_F C_H \alpha_A^2 N_A} \right)^{3/2} \quad (27)$$

decrease as $Q_{\text{cc}} \sim N_A^{-3/2}$. The dashed line in Figure 3 corresponds to the crew-cut asymptote $Q_{3\text{cc}}$, eq 27, with the slope $-3/2$ as indicated. For the chosen set of parameters these asymptotes do not look like a good approximation of full expressions (solid lines in Figures 2 and 3). The range of applicability of this regime is very narrow because the contribution of the core to the free energy of the micelle was ignored in both starlike and crew-cut regimes. However, with decrease of the mass of the corona block this contribution of the core to the free energy of the micelle becomes significant. In addition, the range of the crew-cut spherical regime is narrowed by the transition to the cylindrical morphology.

For the crew-cut morphology, the free energy per chain yields

$$F_{3\text{cc}}/kT = 2\gamma^{1/2} \left(\frac{C_F C_H p_A^{-1/2} \alpha_A^2 N_A}{\alpha_B^2} \right)^{1/2} \quad (28)$$

The corona of a crew-cut micelle can be envisioned as a quasi-planar brush. Similarly to a starlike micelle, a crew-cut micelle is stabilized by the balance of the surface and the corona free energies. Although the corona thickness is less than the core radius, the chains in the corona remain noticeably stretched, and the corona free energy still dominates over the elastic stretching of the core blocks. Asymptotic scaling dependences (25)–(28) are therefore valid when the free energy of elastic stretching of core block B is negligible with respect to the free energy of corona block A . The lower boundary for this regime is expected when all three contributions to free energy, F_{A3} , F_{B3} , and F_{s3} , become on the same order of magnitude. This happens⁴ when the molecular weight of block B reaches the value of N_B^{**}

$$N_B = N_B^{**}(N_A) \approx \varphi^2 p_B p_A^{-3/4} \gamma^{-1/2} N_A^{3/2} \left(\frac{\alpha_A}{\alpha_B}\right)^3 \quad (29)$$

However, as we show in section 4, prior to the onset of the core-stabilized regime (expected at $N_B \gg N_B^{**}$), the spherical micelles rearrange into cylindrical aggregates.

3.2. Cylindrical Micelle. Cylindrical micelles can be modeled by a long cylindrically shaped body with two spherically shaped end-caps. These caps are less favorable than the cylindrical part of the micelle. The difference in the free energies per chain in spherical caps and in cylindrical parts governs the average length of the micelle.²⁹ In the present paper we consider

cylindrical aggregates ($j = 2$) long enough that the contribution of spherical caps decorating both ends of the micelle can be neglected.

Taking into account eqs 1, 6, 8, AI.1a, AI.2a, and AI.18, we represent the free energy of a block copolymer chain in a very long cylindrical micelle as

$$\frac{F_2}{kT} = \frac{\pi^2 r_2^2}{16p_B N_B} + \gamma \frac{2N_B}{\varphi r_2} + \sqrt{2} C_{FP_A}^{-3/4} r_2^{3/2} \frac{\varphi^{1/2}}{N_B^{1/2}} \left[\left(1 + \frac{3}{2\sqrt{2}} \frac{C_{HP_A}^{1/4} \alpha_A^2 N_A \varphi^{1/2}}{\alpha_B^2 r_2^{1/2} N_B^{1/2}} \right)^{1/3} - 1 \right] \quad (30)$$

By minimizing F_2 with respect to r_2 ($\delta F_2 / \delta r_2 = 0$), we arrive at the nonlinear equation that determines the equilibrium value of the dimensionless core radius $r_2 = R_2 / a_B$

$$\frac{\pi^2 r_2}{8p_B N_B} - \gamma \frac{2N_B}{\varphi r_2^2} + \frac{3}{\sqrt{2}} C_{FP_A}^{-3/4} r_2^{1/2} \frac{\varphi^{1/2}}{N_B^{1/2}} \left[\left(1 + \frac{3}{2\sqrt{2}} \frac{C_{HP_A}^{1/4} \alpha_A^2 N_A \varphi^{1/2}}{\alpha_B^2 r_2^{1/2} N_B^{1/2}} \right)^{1/3} - 1 \right] - \frac{C_H C_F}{4} \left(\frac{\alpha_A}{\alpha_B} \right)^2 \left(\frac{\varphi}{N_B} \right)^{p_A - 1/2} \frac{N_A}{\left(1 + \frac{3}{2\sqrt{2}} \frac{C_{HP_A}^{1/4} \alpha_A^2 N_A \varphi^{1/2}}{\alpha_B^2 r_2^{1/2} N_B^{1/2}} \right)^{4/3}} = 0 \quad (31)$$

The numerical solution of this equation is plotted as line 2 in Figure 2a. By substituting r_2 in eq 30, we find the equilibrium free energy per chain in a very long cylindrical micelle.

The thickness of the cylindrical corona H_2 is given by eqs AI.19 and AI.1a

$$H_2 = R_2 \left[\left(1 + \frac{3}{2\sqrt{2}} \frac{C_{HP_A}^{1/4} \alpha_A^2 N_A \varphi^{1/2}}{\alpha_B^2 r_2^{1/2} N_B^{1/2}} \right)^{2/3} - 1 \right] \quad (32)$$

The total radius of the cylindrical micelle R_2^{tot} is

$$R_2^{\text{tot}} = H_2 + R_2 \quad (33)$$

The thickness of the cylindrical corona H_2 is plotted in Figure 2b (line 2). The aggregation number per unit length is the linear density ρ of block copolymer molecules along the cylindrical micelle

$$\rho = \frac{\pi r_2^2 \varphi}{\alpha_B N_B} \quad (34)$$

3.2.1. Asymptotic Dependencies of Cylindrical Micelles. Equations 30–34 determine the equilibrium characteristics of cylindrical micelle for arbitrary values of N_A and N_B . The asymptotic expressions for the core radius R_2 were derived by delineating and balancing the leading terms in the free energy F_2 . We consider the two limiting cases of the bottle-brush ($H_2 \gg R_2$) and the crew-cut ($H_2 \ll R_2$) micelles.

Bottle-Brush Cylindrical Micelle. Similar to starlike spherical micelles, the elastic free energy F_{B2} of core block B can be neglected for a bottle-brush micelle. The thickness of corona H_2 in a bottle-brush micelle is noticeably larger than core radius R_2 . By substituting $\nu = 1/2$ in eq AII.19 and using Θ solvent expressions of

coefficients \hat{C}_H and \hat{C}_F (eqs AI.1a and AI.2a), we arrive at the scaling expression⁴ for the free energy of a bottle-brush cylindrical micelle

$$F_{2\text{bb}}/kT \simeq \gamma^{4/7} \left(\frac{\alpha_A}{\alpha_B} \right)^{2/7} N_A^{1/7} p_A^{-2/7} \left(\frac{N_B}{\varphi} \right)^{2/7} \quad (35)$$

By comparing $F_{2\text{bb}}$ (eq 35) with $F_{3\text{star}}$ (eq 23), we find that for $N_B < N_B^*$ (eq 24) corresponding to the regime with coronas larger than cores (starlike spherical and bottle-brush cylindrical micelles), $F_{3\text{star}} < F_{2\text{bb}}$. Therefore, bottle-brush cylindrical aggregates are thermodynamically unstable with respect to starlike micelles.

Crew-Cut Cylindrical Micelle. For crew-cut cylindrical micelles with $H_2 < R_2$, the situation is different. Here, the free energy per chain in the corona F_{A2} is given by eq AI.17, and it is only slightly different from the free energy per chain F_{A1} in a planar brush. Therefore, the leading terms in the free energy of crew-cut spherical and crew-cut cylindrical micelles coincide and are given by eq 28. By balancing the dominant contribution in F_{A2} (that is, free energy of the planar brush F_{A1}) with the surface energy F_s , we arrive at the equilibrium value of the surface area per chain (eq 26). The respective stability of the aggregates is determined by the corrections to this free energy due to different geometries of the micelles. The decrease of the corona free energy due to the bending of a planar corona into a cylindrical one is less than for a spherically bent corona (see eqs AI.17 and AI.28). Therefore, the crew-cut corona prefers a spherical geometry. However, at the same area per chain the core prefers the cylindrical geometry and the equilibrium morphology depends on the balance of the core and corona free energy differences. The details of the sphere-to-cylinder transition will be discussed in section 4.

For a crew-cut cylindrical micelle, the asymptotic scaling laws for the core radius R_2 and the linear density of block copolymer molecules ρ are given respectively (eqs AI.1a, AI.2a, AII.12, and AII.15 for $\nu = 1/2$) by

$$R_{2\text{cc}} = \frac{2N_B}{\varphi} \frac{\alpha_B^2}{\alpha_A} \left(\frac{\gamma p_A^{1/2}}{C_F C_H N_A} \right)^{1/2} \quad (36)$$

and

$$\rho_{\text{cc}} = 4\pi\gamma \frac{p_A^{1/2}}{C_F C_H} \frac{\alpha_B}{\alpha_A^2} \frac{N_B}{N_A \varphi} \quad (37)$$

As shown in Figure 2a, the crew-cut asymptotic value of the core radius $R_{2\text{cc}}$ (line 6) is 15–35% larger than the numerical solution of eq 31.

The free energies of spherical and cylindrical crew-cut aggregates obey the same scaling laws, and therefore the lower boundary for the crew-cut regime of cylindrical micelles is determined by the same expression as for the spherical micelles (eq 29) up to numerical prefactor. However, prior to the onset of the core-stabilized regime ($N_B \approx N_B^{**}$), cylindrical micelles rearrange into lamellar aggregates, and subsequent precipitation of block copolymer takes place.

3.3. Lamellar Morphology. We consider now a single lamellar bilayer with a condensed core of thickness $2R_1 = 2a_B r_1$ and two planar coronas with area s per chain and thickness H_1 each (Figure 1). Similarly to the case of cylindrical micelles, we ignore the free

energy losses associated with the edges of the bilayer and limit our analysis to a very large planar aggregate.

The free energy per chain in a very large lamellar aggregate (eqs 1, 6, AI.1a, AI.2a, and AI.4) yields

$$\frac{F_1}{kT} = \frac{\pi^2 r_1^2}{8p_B N_B} + \gamma \frac{N_B}{\varphi r_1} + \frac{C_F C_H a_A^2 N_A \varphi r_1}{p_A^{1/2} a_B^2 N_B} \quad (38)$$

By minimizing F_1 with respect to r_1 ($\delta F_1 / \delta r_1 = 0$), we obtain the equation that determines the equilibrium radius (half-width) of the lamella core

$$\frac{\pi^2 r_1}{4p_B N_B} - \gamma \frac{N_B}{\varphi r_1^2} + \frac{C_F C_H a_A^2 N_A \varphi}{p_A^{1/2} a_B^2 N_B} = 0 \quad (39)$$

The equilibrium thickness of the corona (eqs AI.1a and AI.3) yields

$$H_1 = \frac{a_A^2}{a_B} C_H N_A p_A^{1/4} \left(\frac{\varphi}{N_B} \right)^{1/2} r_1^{1/2} \quad (40)$$

whereas surface density of the chains (eq 4)

$$\sigma_1 = \frac{1}{s_1} = \frac{\varphi r_1}{a_B^2 N_B} \quad (41)$$

The core radius $R_1 = r_1 a_B$ and the corona thickness H_1 are plotted in Figure 2a,b (line 1 in both figures).

By substituting the numerical solution r_1 in eq 38, we find the equilibrium free energy per chain in the lamellar aggregate. Let us consider the asymptotic scaling laws for the aggregate dimensions. If block A is long, lamellar aggregates would be thermodynamically unstable with respect to both spherical and cylindrical micelles. The possible stability range of the lamellae is associated with the crew-cut shape of the aggregate ($H_1 < R_1$). We therefore consider only this case.

For crew-cut micelles close to the cylinder-to-lamella transition, the dominant contribution to the free energy, $F_{1cc} \approx F_{A1cc} + F_{s1}$, is given by eq 28. Here the stretching of block B is neglected in comparison with the leading terms. Therefore, the area per chain s_1 is equal to s_{cc} (eq 26), and we arrive at the corresponding scaling law for lamella radius

$$R_{1cc} = \frac{N_B a_B^2}{\varphi a_A} \left(\frac{\gamma p_A^{1/2}}{C_F C_H N_A} \right)^{1/2} \quad (42)$$

As shown in Figure 2a, the crew-cut asymptotic value of the core radius R_{1cc} (line 5) is 20–40% larger than the numerical solution of eq 39 (line 1).

As noted above, surface area s_j is almost the same in crew-cut micelles of all considered morphologies ($s_j = s_{cc}$) and is given by eq 26. Therefore, micelles of different morphologies have almost the same corona thickness ($H_1 \approx H_2 \approx H_3$, or $H_j \approx H_1$), whereas the core radius varies with micelle morphology as $R_j \approx jR_1$, which is the direct consequence of eq 3. Figure 2a,b indicates that in the range of crew-cut micelles (for short corona block N_A) the relations $H_j \approx H_1$ and $R_j \approx jR_1$ are indeed valid (see lines 1, 2 and 3).

3.3.1. Solubility of Lamellae in Solution. Lamellar bilayers in solutions are not perfectly flat but undulate due to thermal fluctuations. Such undulations give rise to the entropic repulsion between bilayers similar to the

Helfrich force between lipid membranes.²⁸ However, because of higher bending rigidity of block copolymer bilayers, the van der Waals attraction between them dominates over the Helfrich repulsion,⁷ and therefore lamellae precipitate from solution. The structure of the sediment was considered in detail in ref 7. Depending on the block copolymer composition, the sediment consists of the lamellar mesophase (stack of parallel lamellae selectively swollen by the solvent) or inverted micelles (where the core of shorter soluble block A is surrounded by the corona of insoluble block B).

We note that the free energy per chain, $F_{1(m)}$, in the lamellar mesophase in the sediment is slightly lower than the free energy per chain, F_1 , for a single bilayer in solution (eq 38) due to the van der Waals attraction energy. The dominant contribution to the van der Waals energy of lamella stack is due to the nearest-neighbor interactions. For the parallel flat stack of crew-cut ($R_1 \gg H_1$) lamellae, the free energy difference $\Delta F_1 = F_1 - F_{1(m)}$ can be estimated as twice the van der Waals energy, F_W , of the two infinitely thick planar slabs (cores of the lamellae) separated by distance $2H_1$ (two corona thicknesses) to give

$$\Delta F_1 = -F_W \approx 2 \frac{As_1}{12\pi(2H_1)^2} \approx \frac{As_1}{24\pi H_1^2} \quad (43)$$

where s_1 is the area per chain in the lamella and A is the Hamaker constant.²⁹ We thus find that for a lamellar mesophase with planar brushlike coronas ($H_1/\sqrt{s_1} > 1$), and a typical value of $A \approx kT$, the shift in the free energy ΔF_1 per chain is quite small, $\Delta F_1 \approx 10^{-2} kT$. Thus, the van der Waals attraction is negligible with respect to the free energy of a block copolymer in the aggregate, $\Delta F_1 \ll F_1$, and cannot affect the polymer conformation. Therefore, the instability and phase separation of block copolymer solution can be delineated from the condition $F_1 = F_2$.³⁰

The structure of the sediment is determined by a hierarchy of different interactions. The dominant interaction is the attraction between B monomers, leading to the aggregation of block copolymer and formation of dense B domains. The next energy scale (still much larger than kT per chain) is the surface and deformation free energies. The free energy per chain, F_j , in a micelle remains much larger than kT . The van der Waals attraction between different aggregates keeps them together in a precipitated microsegregated phase although the van der Waals energy per chain F_W is much smaller than kT . The morphology of the mesophase is determined by the chemical composition of block copolymer.

Recent studies on the conformations of bilayers indicate, however, that the planarlike conformation of the coronas in lamella can be distorted due to flip-flop (redistribution) of block copolymer molecules.^{31–33} Relaxation of the elastic stretching of the corona blocks A due to redistribution of the chains from the inner to the outer part of a curved lamella can lead to a decrease in the total free energy (with respect to the planar conformation) and cause a spontaneous curvature of the bilayer.^{34,35} In this case, the sediment could comprise the distorted lamellar mesophase (locally curved lamellar sheets with the characteristic radius of curvature determined by the block copolymer composition). Our preliminary analysis indicates that in the experimentally relevant range of parameters the free energy per

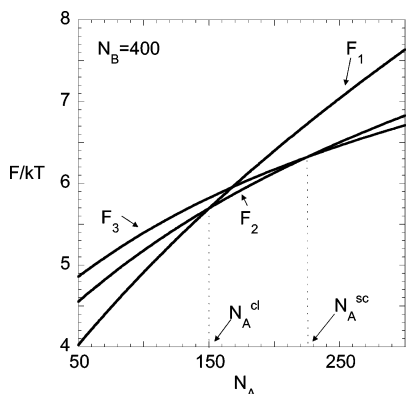


Figure 4. Free energies per chain in lamellar (F_1 , eq 38), cylindrical (F_2 , eq 30), and spherical (F_3 , eq 13) aggregates as functions of the degree of polymerization of the corona block N_A . The vertical dotted lines indicate the cross over from spherical to cylindrical and cylindrical to lamellar micelles. The set of model parameters is the same as in Figure 2.

chain in the curved crew-cut lamella, $F_{1(curv)}$, is only slightly (on the order of a few percent) lower than in a planar bilayer, F_1 . That is, $F_1 - F_{1(curv)} \approx 10^{-2}F_1$, and the free energies in a planar and curved lamellae are almost the same, $F_1 \approx F_{1(curv)}$. Note that the van der Waals attraction for curved lamellae is weaker than for planar ones due to the larger average distance between the sheets and therefore cannot distort the polymer conformation.

Below, we delineate the cylinder-to-lamella transition and the associated instability of the solution by merely equating the free energies per chain in lamellar and cylindrical aggregates, $F_1 = F_2$.

4. Transitions: Sphere–Cylinder–Lamella

By comparing the equilibrium free energies (eqs 13, 30, and 38) of all three different morphologies, we can locate the sphere-to-cylinder and cylinder-to-lamella transitions and determine the ranges of stability of the spherical, cylindrical, and lamellar aggregates. Figure 4 demonstrates typical dependences for the free energies for micelles of the three different morphologies. We choose a typical value of $N_B = 400$ and experimentally relevant set of other model parameters (specified in the legend to Figure 2). For this set of parameters, the free energy of a spherical micelle F_3 is the smallest ($F_3 < F_2 < F_1$) when $N_A > N_A^{sc} \approx 225$, where N_A^{sc} is the intersection point of the free energies of sphere F_3 and cylinder F_2 . When $N_A < N_A^{cl} \approx 150$, where N_A^{cl} is the intersection point of the free energies of cylinder F_2 and lamella F_1 , the lamellar aggregate is most stable ($F_1 < F_2 < F_3$). In the intermediate range of molecular weights, $N_A^{cl} < N_A < N_A^{sc}$, a cylindrical micelle is the optimal one.

Figure 5 demonstrates the ratio of corona thickness H and core radius R as a function of the degree of polymerization of the corona block N_A for micelles of three different morphologies for the same values of model parameters as in Figure 2. While this ratio is much larger than unity in the spherical region for large N_A , it becomes on the order of unity in the transition region. Figure 5 indicates that the change in micelle morphology takes place when spheres and cylinders have a crew-cut structure, that is, when the size H of the corona is less than the core radius R . Here, for the sphere–cylinder transition at $N_A = N_A^{sc} \approx 225$ one finds the size ratio $H_3/R_3 \approx 0.45$. A slightly larger value of

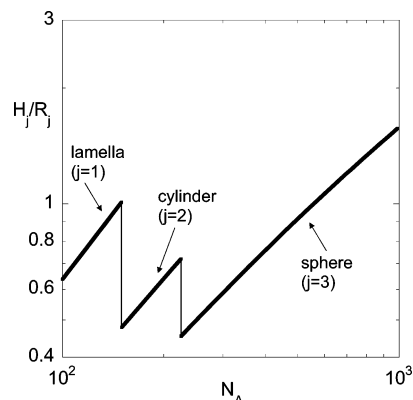


Figure 5. Plot of the ratio of the corona thickness (H_j) and core radius (R_j) in the stability range for the three different morphologies: lamella (1), cylinders (2), and spheres (3). The transition from spherical to cylindrical and cylindrical to lamellar micelles happens in the crew-cut regime when $H_j/R_j < 1$. The set of model parameters is the same as in Figure 2.

$H_2/R_2 \approx 0.48$ is found for the lamella-to-cylinder transition at $N_A = N_A^{cl} \approx 150$. Note that the corona-to-core size ratio H_j/R_j significantly increases during the sphere-to-cylinder and cylinder-to-lamella transitions. This increase is mostly due to the decrease of the core size R_j (Figure 2a), while the thickness of the crew-cut corona H_j increases only slightly (Figure 2b).

Approximations for the boundaries between the different morphologies can be derived using the asymptotic scaling laws obtained in the previous section (see Appendix III). For crew-cut aggregates in a Θ solvent ($\nu = 1/2$), the asymptotic free energy per chain in a micelle of morphology $j = 1, 2$, and 3 can be represented as

$$\frac{F_{1cc}}{kT} \approx 2\gamma^{1/2} \left(\frac{C_F C_H p_A^{-1/2} a_A^2 N_A}{a_B^2} \right)^{1/2} + \frac{\pi^2}{8} \frac{r_1^2}{p_B N_B} \quad (44)$$

$$\frac{F_{2cc}}{kT} \approx 2\gamma^{1/2} \left(\frac{C_F C_H p_A^{-1/2} a_A^2 N_A}{a_B^2} \right)^{1/2} - \frac{1}{2} C_F p_A^{-3/4} \frac{a_A^2 h_1^2}{a_B \sqrt{s_2} r_2} + \frac{\pi^2}{16} \frac{r_2^2}{p_B N_B} \quad (45)$$

$$\frac{F_{3cc}}{kT} \approx 2\gamma^{1/2} \left(\frac{C_F C_H p_A^{-1/2} a_A^2 N_A}{a_B^2} \right)^{1/2} - C_F p_A^{-3/4} \frac{a_A^2 h_1^2}{a_B \sqrt{s_3} r_3} + \frac{3\pi^2}{80} \frac{r_3^2}{p_B N_B} \quad (46)$$

where $s_j = s_{cc}$ is given by eq 26 for all three morphologies and $r_j = r_{jcc} = (jN_B a_B^2)/(\varphi s_{cc})$. The first (dominant) term in eqs 44–46 results from the balance of the surface free energy and the free energy of the planar corona. It is given by eq 28 and is the same for spheres, cylinders, and lamellae because the surface area per chain is almost the same in all three morphologies. The second (negative) terms in eqs 45 and 46 are the corrections to the free energy of planar corona due to curvature in cylindrical (eq AI.17) and spherical (eq AI.28) geometries. Finally, the last terms in eqs 44–46 are the elastic free energies of the core block B (eqs 6 and 7).

The sphere-to-cylinder transition is specified by $F_{3cc} = F_{2cc}$ and taking into account eqs 26 and AI.3. The

asymptotic boundary between micellar phases with spherical and cylindrical morphologies is given by eqs AIII.8, AI.1a, and AI.2a

$$N_A^{\text{sc}} \approx \left(\frac{21\pi^2}{20}\right)^{4/11} C_F^{-7/11} C_H^{-1} \left(\frac{\alpha_B}{\alpha_A}\right)^2 p_A^{5/22} p_B^{-4/11} \gamma^{3/11} \varphi^{-12/11} N_B^{8/11} \quad (47)$$

A similar scaling dependence was obtained for the boundary between cylindrical and lamellar morphologies by equating $F_{1\text{cc}} = F_{2\text{cc}}$ (eqs 44 and 45); see eq AIII.9 with eqs AI.1a and AI.2a

$$N_A^{\text{cl}} \approx \left(\frac{\pi^2}{2}\right)^{4/11} C_F^{-7/11} C_H^{-1} \left(\frac{\alpha_B}{\alpha_A}\right)^2 p_A^{5/22} p_B^{-4/11} \gamma^{3/11} \varphi^{-12/11} N_B^{8/11} \quad (48)$$

The only difference between eqs 47 and 48 is the numerical coefficient, which is smaller for the cylinder–lamellar boundary. Clearly, the calculated scaling boundaries eqs 47 and 48 are located in the regime of crew-cut micelles. Equations 47 and 24 indicate that for copolymers with $p_A \approx p_B \approx 1$, $N_B^{\text{sc}}/N_B^* \gg 1$ when

$$N_A \gg N_A^\circ \approx \frac{\gamma K^2 (\alpha_B)^{42}}{\varphi^4 (\alpha_A)^{42}} \quad (49)$$

Here N_A° is the degree of polymerization of soluble blocks above which micelles have a crew-cut structure when they undergo the morphological transitions (the ratio $H_j/R_j < 1$). For shorter chains ($N_A < N_A^\circ$) the transitions occur in the starlike regime. Using typical experimental parameters given in Tables 1 and 2, for sample 4, the spherical micelle sample closest to the transition to cylinders, one calculates $N_A^\circ = 0.9$. Since the value $N_A = 244$ for sample 4 is much larger than 0.9, the transition clearly takes place in the crew-cut regime.

We therefore find that in the limit of large molecular weights of the blocks the sphere-to-cylinder transition as well as precipitation of the micelles associated with the cylinder-to-lamella transition occurs when aggregates have a crew-cut structure, and the parameters of micelles

are determined by the balance between the free energy of a planarlike corona and the surface free energy.

We note, however, that more precise calculations of the boundaries and of the ratio H/R (Figures 4 and 5) indicate that in the experimentally relevant range of N_B the ratio H/R at transition value of N_A^{sc} can be close to unity in the cylindrical morphology. For example, for $N_B = 400$, the ratio $H_2/R_2 \approx 0.72$ at the transition value of $N_A = N_A^{\text{sc}} \approx 225$ where the spherical micelle transforms into the cylindrical aggregate. That is, in experimentally accessible range $N_B \approx 400$, a cylindrical micelle at the transition point can be found near the boundary between the bottle-brush and the crew-cut regimes. The corona of lamella at the transition point $N_A = N_A^{\text{cl}} \approx 150$ is slightly larger than the core ($H_1/R_1 \approx 1.01$).

The approximate expressions for the boundaries (eqs 47 and 48) in the limit of large molecular weight of the blocks give the correct value of the exponent, $N_A^{\text{sc}} \sim N_A^{\text{cl}} \sim N_B^{8/11}$ (see below), and provide reasonable estimates for the transition points and stability ranges of micelles with different morphologies. In particular, eqs 47 and 48 allow us to estimate the width of the cylindrical phase (an interval of degrees of polymerization ΔN_A of corona block, where cylindrical micelles are thermodynamically stable). According to eqs 47 and 48, the ratio

$$\frac{\Delta N_A}{N_A^{\text{cl}}} = \frac{N_A^{\text{sc}} - N_A^{\text{cl}}}{N_A^{\text{cl}}} \approx \left(\frac{21\pi^2}{20} \frac{2}{\pi^2}\right)^{4/11} - 1 \approx 0.31 \quad (50)$$

is asymptotically independent of block copolymer parameters (see eq AIII.10). A more precise calculation of the boundaries gives a larger value of $\Delta N_A/N_A^{\text{cl}} \approx 225/150 - 1 \approx 0.50$ for the insoluble block with $N_B = 400$ monomers. An increase in N_B leads to the decrease in $\Delta N_A/N_A^{\text{cl}}$ and gradual approach to the asymptotic value 0.31 given by eq 50 (for example, for $N_B = 10^6$, $\Delta N_A/N_A^{\text{cl}} \approx 0.38$). Below we compare these predictions with the experimentally measured stability range of cylindrical micelles and find a reasonable agreement with the experimental value $\Delta N_A/N_A^{\text{cl}} \approx 0.37$ (see section 5).

5. Comparison with Experiment

We compare our predictions with recent experimental results on polystyrene–polyisoprene (PS-*b*-PI) block copolymer that forms micelles in the selective solvent

Table 1. Equilibrium Characteristics of PS–PI Diblocks in Heptane

no.	N_{PS}^a	N_{PI}^a	Q^b	R_h (Å) ^c	R_{core} (Å) ^d	φ^e	ρ (Å ⁻¹) ^f	type ^g
1	393	1443	120 ± 5	542 ± 5	157 ± 5	0.5 ± 0.08		sph
2	393	797	149 ± 7	446 ± 2	158 ± 6	0.6 ± 0.08		sph
3	393	412	292 ± 8	363 ± 3	186 ± 8	0.7 ± 0.12		sph
4	393	244	339 ± 11	319 ± 6				sph
5	342	272	219 ± 10	291 ± 4				sph
6	342	222	274 ± 9	285 ± 2				sph
7	342	188	330 ± 7	270 ± 5				sph
8	393	210						sph/cyl
9	393	184						cyl
10	393	181						cyl
11	393	179						cyl
12	392	153			165 ± 7	0.7 ± 0.12	0.8 ± 0.2	cyl
13	393	151						insoluble
14	393	147						insoluble

^a The degree of polymerization of the polystyrene (polyisoprene) block was determined as $N_{PS} = M_{PS}/104$ ($N_{PI} = M_{PI}/68$), where M_{PS} (M_{PI}) is the molecular weight of the polystyrene (polyisoprene) block and $M = 104$ ($M = 68$) is the molecular weight of the corresponding monomeric unit. ^b Aggregation number of spherical micelles. ^c Hydrodynamic radius of spherical micelles from SLS. ^d Radius of the core from neutron scattering. ^e Volume fraction of the polystyrene block in the core. ^f Linear density (number of chains per unit length) of cylindrical micelles. ^g Micellar morphology as observed by SLS and AFM.

Table 2. Parameters of the Theoretical Model

a_A	a_B	p_A	p_B	φ	$\gamma/\varphi^{2/3}$	C_F	C_H
5.0 Å	5.6 Å	1.6	1.5	0.7	0.097	1.38	0.68

heptane¹³ (see Table 1). Even though heptane is a moderately good solvent for PI, its solubility properties are close to Θ solvent. This makes the size of the largest corona blob smaller than thermal blob. Therefore, in the main part of the paper we use equations of the Appendices for Θ solvents with exponent $\nu = 1/2$. Depending on the values of the molecular weights of the blocks, micelles of spherical or cylindrical morphologies as well as insoluble sediment were detected in solutions. For spherical micelles, static light scattering (SLS) and dynamic light scattering (DLS) techniques provided aggregation number Q and hydrodynamic radius R_h .²⁴ For cylindrical micelles, independent measurements of linear density ρ of block copolymer along the micellar contour were carried out by atomic force microscopy (AFM) and static light scattering (SLS).¹⁴ Small-angle neutral scattering (SANS) and small-angle X-ray scattering (SAXS) studies were performed to measure the core radii R of spherical and cylindrical micelles. The results of these experiments are summarized in Table 1.

We first use the handbook data to determine the monomer sizes a_A , a_B and the stiffness parameters p_A , p_B for polyisoprene (PI) and polystyrene (PS). Then we delineate the values of surface tension of polystyrene in heptane γ and volume fraction φ in the core of micelles from the literature data. Finally, we determine the values of numerical coefficients C_H and C_F by fitting the predicted theoretical dependences with the experimental data on spherical micelles of PS–PI diblock copolymer in heptane. The same set of parameters will be used to predict the properties of cylindrical micelles and to compare these predictions with our experimental data.

5.1. Values of Model Parameters.

5.1.1. Monomer Size a and Stiffness Parameter p of the Blocks. We estimate monomer size a and stiffness parameter p for soluble block A (polyisoprene) and insoluble block B (polystyrene) by the following procedure. We represent each monomer as a cube of size a with volume $V_0 = a^3$. Using the relationship $V_0 = M_0/(\rho_{\text{bulk}}N_{\text{Av}})$, where M_0 is the molar mass of a monomer (in g/mol), ρ_{bulk} is the polymer bulk density, and N_{Av} is Avogadro's number, we find

$$a = V_0^{1/3} = \left(\frac{M_0}{\rho_{\text{bulk}}N_{\text{Av}}} \right)^{1/3} \quad (51)$$

We substitute the values $M_0 = 68$ g/mol, $\rho_{\text{bulk}} \approx 0.9$ g/mL for PI block and $M_0 = 104$ g/mol, $\rho_{\text{bulk}} \approx 1.0$ g/mL for PS block to get

$$a_A \approx 5.0 \text{ \AA} \quad \text{and} \quad a_B \approx 5.6 \text{ \AA} \quad (52)$$

To determine the value of stiffness parameter p for each block, we use the experimental value of the reduced mean-square end-to-end distance in a Θ solvent, $C_\infty = R_0^2/M$, where M is the molar mass of the polymer. From the definition of the stiffness parameter (dimensionless analogue of C_∞) $p \equiv R_0^2/(Na^2)$ where $N = M/M_0$ is the number of monomers, we obtain

$$p = \frac{C_\infty M_0}{a^2} \quad (53)$$

We substitute the values from ref 36 of $C_\infty \approx 0.60$ Å²mol/g for PI block and $C_\infty \approx 0.43$ Å²mol/g for PS block and using values of a_A and a_B from eq 52 and find

$$p_A \approx 1.6 \quad \text{and} \quad p_B \approx 1.5 \quad (54)$$

5.1.2. Excluded-Volume Parameter v . The value of the excluded-volume parameter v determines the thermodynamic quality of the solvent (heptane) for the corona block (PI). It can be obtained from static light scattering (SLS). This technique provides the value of the second virial coefficient A_2 of polymer–polymer interaction in the dilute solution. Experiments were performed for a polyisoprene sample with molecular weight 3.4×10^5 g/mol, yielding the value of $A_2 = (4.1 \pm 0.3) \times 10^{-4}$ cm³ mol/g². By using the relationship² $v = 2A_2M_0^2/(a_A^3N_{\text{Av}})$, we find

$$v \approx 0.05$$

Substituting $a_A = 5$ Å, $p_A = 1.6$, and $v = 0.05$ into the expression for the thermal blob size $\xi_t \approx a_A p_A^2 v^{-1}$, we estimate $\xi_t \approx 260$ Å. The largest blob in the corona is the last blob in the spherical starlike micelle with the largest soluble block with degree of polymerization $N_A \approx 1443$ (sample 1 in Table 1). Its size ξ_{last} can be estimated as

$$\xi_{\text{last}} = \frac{R_3^{\text{tot}}}{\sqrt{Q}} p_A^{3/4} \quad (55)$$

By calculating the size R_3^{tot} (eq 16) and aggregation number Q (eq 17) for sample 1, we find $\xi_{\text{last}} \approx 70$ Å. Because $\xi_t > \xi_{\text{last}}$, the excluded-volume interactions do not significantly modify the chain conformation. Therefore, chain conformations in all other (smaller) blobs in spherical, cylindrical, and lamellar micelles are also Gaussian. Thus, despite the positive value of second virial coefficient A_2 , heptane is apparently a Θ solvent for PI block in the micellar corona wherein all correlation blobs are smaller than the thermal blob.

5.1.3. Dimensionless Surface Tension γ and Volume Fraction φ of Polymer in Micellar Core. As noted earlier, the dimensionless surface tension γ and volume fraction φ are not independent variables. Both parameters depend on the solvent quality. For weakly poor solvent for B block, the relatively small value of polymer volume fraction φ in the core of the micelle is determined by the ratio of the attractive second and the repulsive third virial coefficients of monomer–monomer interactions. The dimensionless surface free energy γ can be approximated in the range of small $\varphi \ll 1$ as $\gamma = \gamma_1 \varphi^2$.^{1,2} (Here, γ_1 is the numerical coefficient on the order of unity.) However, at relatively high polymer concentrations higher-order interactions become significant, and simple scaling models fail. Therefore, to facilitate comparison between theory and experiment, we do not make a priori assumptions about the relationship between γ and φ at high values of $\varphi \lesssim 1$ but try to estimate them independently of each other from different experiments.

A convenient method to evaluate γ was proposed in ref 24. The static light scattering (SLS) technique was used to examine solutions of PS in heptane and to determine the solubility of PS as a function of temperature and molecular weight. Heptane is a poor solvent for PS, and the solution separates into a denser phase (sediment) with polymer concentration φ and a dilute

phase that contained individual globules of collapsed PS. The equilibrium concentration φ' of polymer in the dilute phase was determined from the light scattering data for PS samples with three different molecular weights. The chemical potential of a globule in the dilute phase, μ_g , was approximated as

$$\mu_g \approx kT \ln(\varphi'/N_B) + F_{s0} + F_0 \quad (56)$$

where $F_{s0} \sim kT\gamma N_B^{2/3}$ is the surface free energy of the globule, eq 10, and F_0 is the free energy per chain of monomer–monomer interactions in the condensed state. The chemical potential of polymer in the sediment is dominated by the bulk while the surface contribution is negligible. This gives

$$\mu_p \approx kT \ln(\varphi/N_B) + F_0 \quad (57)$$

Equilibrium between dilute phase and sediment implies equality of chemical potentials, $\mu_g = \mu_p$. Therefore, concentrations in the two phases, φ and φ' , are related through the equation

$$\ln(\varphi') - \ln(\varphi) + (36\pi)^{1/3} \gamma (N_B/\varphi)^{2/3} = 0 \quad (58)$$

Assuming that polymer volume fraction in the sediment $\varphi \lesssim 1$ and $\varphi \gg \varphi'$, we omit $\ln(\varphi)$ in eq 58. Then the ratio $\ln(\varphi')/N_B^{2/3}$ is expected to be independent of the molecular weight of polymer N_B and to depend only on temperature T . The data in ref 24 indicated that, for all three molecular weights investigated, the dependence of $\ln(\varphi')/N_B^{2/3}$ on temperature can be approximated by a single straight line, $(0.68 \pm 0.01) - (5.2 \pm 0.2) \times 10^{-3}(T - 273)$, where T is the absolute temperature. We can therefore calculate the ratio $\gamma/\varphi^{2/3}$ from eq 58 as

$$\begin{aligned} \frac{\gamma}{\varphi^{2/3}} &= \frac{(0.68 \pm 0.01) - (5.2 \pm 0.2) \times 10^{-3}(T - 273)}{(36\pi)^{1/3}} \\ &= (0.14 \pm 0.002) - (1.07 \pm 0.04) \times 10^{-3}(T - 273) \end{aligned} \quad (59)$$

Micellar solutions were prepared following the procedure described in detail in refs 13–15. The solutions were equilibrated (annealed) at 60 °C and afterward gradually cooled. The measurements were performed at room temperature. We anticipate that freezing of micelles (lack of micelle equilibration in response to the temperature variation) occurs somewhere between 20 and 60 °C. In our comparison of the theory with experimental data at room temperature, we choose the value of

$$\gamma/\varphi^{2/3} \approx 0.097 \quad (60)$$

corresponding to the freezing temperature $T - 273 \approx 42$ °C.

Equation 60 provides the ratio of two unknown parameters γ and $\varphi^{2/3}$. The values of polymer volume fraction φ in the micellar core of samples 1–3 and 11 were estimated from neutron scattering experiments that measure the core radius R_{core} of spherical (samples 1–3) and cylindrical (sample 11) micelles. If both the aggregation number Q and the core radius R_{core} are known, the polymer volume fraction φ in the core of a spherical micelle is given by $\varphi_{\text{sph}} = (3QN_B V_0)/(4\pi R_{\text{core}}^3)$, where Q was determined from the SLS experiment. The

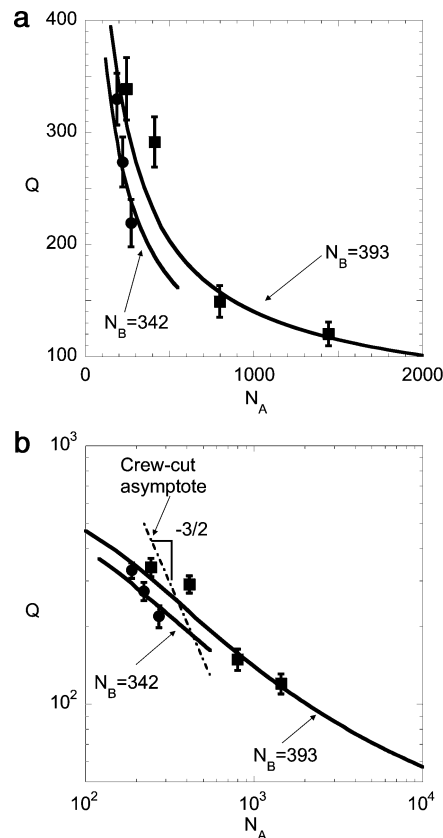


Figure 6. (a) The aggregation number Q (eq 17) for spherical micelle as a function of N_A (the degree of polymerization of the corona block). The circles and squares are experimental data with $N_B = 342$ and 393, respectively. (b) The same dependence is plotted in double-logarithmic coordinates. Theoretical calculations are shown by solid lines, and experimental data are indicated by symbols. Circles are for $N_B = 342$. Squares are for $N_B = 393$. The dashed–dotted line is the crew-cut asymptote (eq 27) with a slope of $-3/2$. The set of model parameters is the same as in Figure 2.

volume fraction in the core of a cylindrical micelle is calculated as $\varphi_{\text{cyl}} = (\rho N_B V_0)/(\pi R_{\text{core}}^2)$, where ρ is the linear density from SLS and AFM experiments.¹⁴ The measured values of polystyrene volume fraction φ in the core are in the range of $\varphi = 0.5$ – 0.7 . To facilitate the comparison between theory and experiment, we choose $\varphi = 0.7$ as the representative value. Note that for polymer volume fraction $\varphi = 0.7$ the logarithmic correction $\ln(\varphi)$ omitted previously in eq 58 does not affect the ratio $\gamma/\varphi^{2/3}$ in eq 59 (the difference is within the experimental error).

We emphasize that the uncertainty in some of the experimental measurements (e.g., φ) gives us certain freedom in choosing the specific values of the corresponding model parameters. Under these conditions, the choice is dictated by a better fit between theory and experiment. More precise experiments would provide us with a more stringent test of the model. At this point, there are still two unspecified dimensionless parameters, C_H and C_F (numerical coefficients in eqs AI.1a and AI.2a expected to be on the order of unity). From comparison with experiments we fix the values of $C_F = 1.38$ and $C_H = 0.68$. All parameters of the theoretical model are summarized in Table 2.

5.2. Aggregation Number of Spherical Micelles. We start our comparison of experimental results and the theory with the aggregation number Q for spherical micelles. Solid lines in Figure 6a demonstrate the

theoretical dependences calculated using eqs 14 and 17 for the values of model parameters specified in the previous subsection (Table 2). The experimental data with error bars for the seven block copolymer samples 1–7 in Table 1 are shown. Samples 1–4 (squares) have the number of monomers in the insoluble block $N_B = 393$, whereas block B for samples 5–7 (circles) is slightly smaller ($N_B = 342$). For chosen values of the model parameters, the agreement between the theoretical predictions (solid lines) and the experimental values of aggregation number Q (symbols) is rather good.

The theoretical estimates indicate that block copolymers with large soluble block A (samples 1 and 2 in Table 1) form starlike micelles, whereas copolymers with shorter block A (samples 3–7 in Table 1) give rise to the crew-cut micelles. Usually, experimental data are plotted in the logarithmic coordinates to check the values of exponents predicted for micelles. Keep in mind that an asymptotic power law dependence of the aggregation number Q on the degree of polymerization of the soluble block N_A exists only for crew-cut micelles (eq 27), while for starlike micelles this dependence is more complicated (eq 22) (see also Figure 3). Figure 6b presents the data from Figure 6a in the logarithmic coordinates. It allows determination of the apparent exponent d ($\log Q/d$) as a function of the degree of polymerization of the corona block N_A . However, the difference between the apparent and the predicted exponent for crew-cut micelle is expected to be large because the range of crew-cut micelles is very narrow. Most of the crew-cut samples fall in the crossover region between starlike and crew-cut micelles. Therefore, accurate comparison between theory and experiment in a wide range of molecular weight of blocks demands full expression for aggregation number Q rather than the scaling asymptotes.

5.3. Hydrodynamic Radius of Spherical Micelles.

To compare our prediction of the total radius of the spherical micelle R_3^{tot} (eq 16) with hydrodynamic radius measured by dynamic light scattering (DLS), we need to estimate the theoretical hydrodynamic radius of the micelle. Hydrodynamic interactions in a semidilute polymer solution are screened on the same length scale as the intermolecular interactions.¹ This implies that the hydrodynamic screening length is on the order of the solution correlation length (blob size ξ). Therefore, the solvent drains through the polymer only on the scale of the last (external) blob of the corona, and R_h is defined as

$$R_h = R_3^{\text{tot}} - C_\xi \xi_{\text{last}} \quad (61)$$

where C_ξ is a numerical coefficient on the order of unity and ξ_{last} is the size of the last (external) corona blob, eq 55. Below we keep $C_\xi = 1$.

Figure 7 demonstrates the theoretical dependences of R_h calculated according to eqs 16 and 61 (solid lines) and experimental values of R_h (symbols). It also shows the theoretical dependences for the total radius R_3^{tot} (dashed lines). Clearly, the correction due to the last (draining) blob is small since the hydrodynamic radius R_h is close to the R_3^{tot} . For starlike micelles with long soluble block A , $R_3^{\text{tot}} \approx H_{\text{star}} \sim N_A^{1/2} K^{-3/10}$ (eq 21). In the experimentally relevant range, it is still important to keep the logarithmic correction K . As shown in Figure 7, the analytical solution and experimental data have

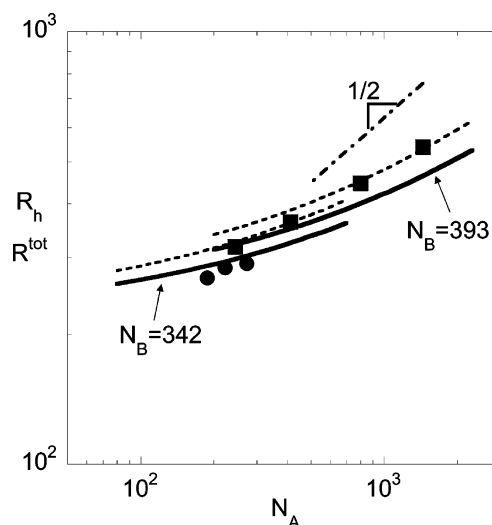


Figure 7. Hydrodynamic radius R_h (solid lines, eq 61) and total micelle radius R_3^{tot} (dashed lines, eq 16) of a spherical micelle as a function of molecular weight N_A of soluble block. Experimental data are shown by symbols. Circles are for $N_B = 342$. Squares are for $N_B = 393$. The dashed-dotted line indicates the exponent of $1/2$ predicted for a starlike micelle in a Θ solvent if the logarithmic term is ignored, i.e., $K = 1$. The set of model parameters is the same as in Figure 2.

a smaller slope than $1/2$ (dotted-dashed line) which is calculated when the logarithmic correction is ignored.

For crew-cut spherical micelles, $R_3^{\text{tot}} \approx R_{3\text{cc}} + H_1(s_{\text{cc}})$ (eqs 25, 26, and AI.3), and there is no power law asymptote for the hydrodynamic radius R_h . Here, an increase in the degree of polymerization of soluble block (N_A) leads to the decrease in the core radius $R_{3\text{cc}} \sim N_A^{-1/2}$ (eq 25 and Figure 2a) and simultaneous increase in the thickness $H_1(s_{\text{cc}})$ of the quasi-planar corona as $H_1(s_{\text{cc}}) \sim N_A^{3/4}$ (eqs AI.3, 26, and Figure 2b). As a result, the total micelle size R_3^{tot} increases only slightly. Figure 7 indicates that the theoretical calculation for R_h is in reasonable agreement with the experimental data.

So far we have analyzed two independently measured characteristics of spherical micelles: aggregation number Q and hydrodynamic radius R_h . We demonstrated that for the chosen set of values of model parameters (Table 2) the experimental data on spherical micelles are in good agreement with the theoretical predictions. Using the same values of model parameters, we now focus on cylindrical micelles.

5.4. Cylindrical Micelles. The presence of giant cylindrical micelles in solution was detected by static light scattering (SLS) and atomic force microscopy (AFM) techniques¹⁴ for samples 8–12 in Table 1. The average contour length of cylindrical micelles $L \approx 4 \times 10^4 \text{ \AA}$ is 2 orders of magnitude larger than their diameter, and therefore the effect of the spherical cups at the ends of these long cylindrical micelles can indeed be neglected. The polymer linear density ρ (the number of molecules per unit length of cylinder defined by eq 34) measured by SLS is $\rho = 0.8 \pm 0.2 \text{ \AA}^{-1}$, while AFM gave $\rho = 0.96 \text{ \AA}^{-1}$. An independent neutron scattering study measured the radius of the core of cylindrical micelle in solution, $R_{\text{core}} \approx 165 \pm 7 \text{ \AA}$.

Using the values of model parameters established earlier for spherical micelles, we calculate core radius R_2 from eq 31 and linear density ρ (eq 34) for samples 8–12 in Table 1

$$R_2 = 132\text{--}142 \text{ \AA} \quad \text{and} \quad \rho \approx 0.55\text{--}0.65 \text{ \AA}^{-1} \quad (62)$$

Clearly, we find a good correspondence between the theoretical and experimental values of core radius R_{core} and linear density ρ , though the theoretical values are slightly lower than the experimental ones.

5.5. Sphere-to-Cylinder and Cylinder-to-Lamella Transitions. By equating free energies $F_3 = F_2$ and $F_2 = F_1$ (eqs 13, 30, and 38), we find the degrees of polymerization N_A^{sc} and N_A^{cl} of corona block A corresponding to the sphere-to-cylinder and cylinder-to-lamella morphological transitions (see section 4 and Appendix III).

Figure 8a demonstrates the theoretical diagram of states for different degrees of polymerization of soluble, N_A , and insoluble, N_B , blocks in logarithmic coordinates. The experimental data are shown by symbols. The regions corresponding to spherical (S), cylindrical (C), and lamellar (L) micelles are separated by the boundaries $N_A^{\text{sc}}(N_B)$ and $N_A^{\text{cl}}(N_B)$, marked by the solid lines. An additional line obtained from the condition $R_3 = H_3$ (dotted line) corresponds to the crossover between regimes of spherical starlike and spherical crew-cut micelles with an asymptotic slope of 4/5 (eq 24). Approximate expressions for the boundaries, N_A^{sc} and N_A^{cl} (eqs 47 and 48), are shown by dashed lines with the slope 8/11. We recall that these boundaries were derived under the assumption that in the transition zone micelles of all morphologies have the crew-cut structure (the corona thickness is smaller than the core radius). In the considered range of $N_B \geq 400$, numerically calculated phase boundaries N_A^{sc} and N_A^{cl} demonstrate the scaling relation $N_A^{\text{sc}} \sim N_A^{\text{cl}} \sim N_B^{0.72}$, which is in excellent agreement with the corresponding asymptotic relation $N_A^{\text{sc}} \sim N_A^{\text{cl}} \sim N_A^{8/11}$ (eqs 47 and 48). Clearly, the asymptotic expressions (eqs 47 and 48) give a good approximation for the stability ranges of different micelles.

The delineated (rectangular) region of the diagram (Figure 8a) is presented separately in Figure 8b to show the more detailed comparison of experimental data with the theoretical diagram of states. Numerically calculated and asymptotic boundaries between micelles of different morphologies are indicated in Figure 8b by the solid and the dashed lines, respectively. The experimental data are marked by squares for spherical micelles (samples 1–8), triangles for cylindrical aggregates (samples 8–12), and diamonds for precipitated samples 13 and 14 (presumably lamellar mesophase in the sediment). Sample 8 with $N_A = 210$ shows the coexistence of spherical and cylindrical micelles. Figure 8b indicates that theory accurately captures the locations of both sphere-to-cylinder and cylinder-to-lamella transitions. The width of the stability range of cylindrical micelles is slightly overestimated by the numerical solution (solid lines) and is underestimated by the approximate expressions 47 and 48 (dashed lines) for S–C and C–L boundaries. The experimental stability range of cylindrical micelles can be obtained from the data for samples 8–12. Sample 12 with $N_A = 153$ has the shortest soluble block A from the series that forms stable cylindrical micelles. Therefore, the experimental stability range of cylindrical micelles is given by $\Delta N_A/N_A^{\text{cl}} = 210/153 - 1 \approx 0.37$. We therefore find a reasonable agreement between the theoretical and the experimental estimates for the stability range of cylindrical

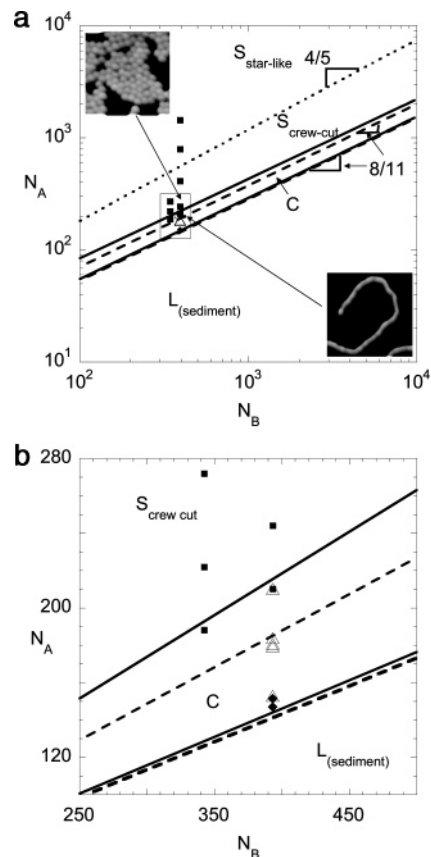


Figure 8. (a) Theoretical diagram of states in logarithmic N_A , N_B coordinates. The crossover boundary between starlike and crew-cut spherical micelles is indicated by the dotted line. The morphological boundaries $N_A^{\text{sc}}(N_B)$ between spherical and cylindrical (eq AIII.8) and $N_A^{\text{cl}}(N_B)$ between cylindrical and lamellar (eq AIII.9) aggregates are shown by solid lines. Asymptotic dependencies of $N_A^{\text{sc}}(N_B)$ and $N_A^{\text{cl}}(N_B)$ from eqs 47 and 48 are indicated by the dashed lines. Samples with spherical micelles are marked by squares, samples with cylindrical micelles are indicated by triangles, and insoluble samples are shown by diamonds. The set of model parameters is the same as in Figure 2. (b) Experimental diagram of states in N_A , N_B coordinates. Samples with spherical micelles are marked by squares, samples with cylindrical micelles are indicated by triangles, and insoluble samples are shown by diamonds. Theoretical boundaries are shown by solid (exact numerical calculation) and dashed lines (asymptotic expressions from eqs 47 and 48). The set of model parameters is the same as in Figure 2.

aggregates. The experimental value $\Delta N_A/N_A^{\text{cl}} \approx 0.37$ is found between the asymptotic $\Delta N_A/N_A^{\text{cl}} \approx 0.31$ and numerical $\Delta N_A/N_A^{\text{cl}} \approx 0.50$ theoretical values.

6. Conclusions

In this study we have developed a theory that describes association of neutral diblock copolymer into micelles in a dilute solution with selective solvent. In these micelles the insoluble block forms a dense core surrounded by a corona of the soluble block. If the corona thickness is larger than the core radius, the micelles are called hairy or starlike; otherwise, if the corona is thinner than the core, the micelles are of the crew-cut type. We compared the free energies of three different morphologies (spherical, cylindrical, and lamellar) and delineated the ranges of their thermodynamic stability. The free energy of a micelle in a selective solvent includes three conventional ingredients: the

surface free energy of the core, the corona free energy, and the elastic stretching of core blocks. For equilibrium micelles of different morphologies the first two terms are large and dominate the free energy. Even for crew-cut micelles with relatively short corona blocks, the elastic contribution of the core remains small compared to the surface and corona free energies; however, it becomes important in determining the transitions between different morphologies.

The free energy of the corona always prefers spherical morphology which provides more space for swollen corona block. The difference in free energy of corona between spherical and other morphologies is large (on the order of the total free energy) for starlike micelles. Therefore, hairy micelles are always spherical. In crew-cut micelles, the energy difference becomes smaller than the total free energy; however, it remains larger than the elastic free energy of the core. Thus, we demonstrate the existence of spherical crew-cut micelles with the thickness of the corona smaller than the radius of the core. For this reason, in most experiments one observes spherical micelles in a wide range of block lengths even for corona blocks considerably shorter than the core block.

The size of starlike micelles is dominated by the corona thickness H_3 which increases as a power law of the degrees of polymerization of the corona and core blocks, N_A and N_B respectively (eq 21). The core radius (R_3) also increases with N_B as a power law and weakly decreases with N_A (eq 18). Similar behavior was predicted and observed for the aggregation number Q , which increases with N_B and decreases only weakly with N_A (eq 22). We demonstrated that this weak logarithmic dependence of Q on N_A is essential for interpretation of experimental data obtained for spherical starlike micelles (see Figure 6). Our findings indicate that the hydrodynamic radius can be approximated by the total micellar radius $R_h \approx R_3^{\text{tot}}$ and that it is necessary to include the logarithmic corrections to describe the experimental data (see Figure 7).

For shorter soluble blocks the thickness of the corona becomes smaller than the radius of the core and one enters the crew-cut region. In this region the asymptotic dependence for aggregation number Q of crew-cut spherical micelles is not relevant, and the full expression for Q should be used. This is a result of the corona in crew-cut spherical micelles being only slightly smaller than the core for the experimentally accessible range of molecular weights. This causes the crew-cut asymptotic description to not be valid. The stability range of spherical crew-cut micelles is rather narrow ($N_B^{8/11} < N_A < N_B^{4/5}$, see Figure 8a) and weakly increases with an increase in molecular weight of the core block N_B . Therefore, in experimentally relevant range of parameters, a proper description of the crew-cut micelles and the transition to the cylindrical morphology cannot be attained by using simple scaling asymptotes (that follow from the dominant contributions to the free energy).

In this work, we accounted not only for the dominant contributions to the micelle free energy but retained also the correction terms of the next order of magnitude. As a result, we were able to describe more accurately the free energy of micelles and delineate the transitions between micelles of different morphologies. We demonstrated that, in the limit of large molecular weights of blocks $N_B \gg N_B^{**}$ (N_A) and $N_A \gg N_A^\circ$ (eqs 29 and 49), the sphere-to-cylinder transition takes place when the

micelles have a crew-cut shape, that is, when the thickness of corona H is noticeably smaller than the size of the core R , $H \ll R$. This is in contrast to the conclusion in earlier investigation⁷ where this transition was predicted to occur at the boundary between the starlike and the crew-cut regimes, that is, when the thickness of the corona is approximately equal to the core radius, $H \approx R$. We found that the sphere-to-cylinder transition occurs at shorter length of corona block A , deep in the crew-cut regime (see Figure 8a). In a Θ solvent, the degree of polymerization N_A^{sc} of block A corresponding to the sphere-to-cylinder transition increases with N_B of the core block as $N_A^{\text{sc}} \sim N_B^{8/11}$. In a good solvent, $N_A^{\text{sc}} \sim N_B^{2/3}$ (see Appendix III). This is a weaker dependence than $N_A^{\text{sc}} \sim N_B^{11/15}$ predicted in ref 7 for the good solvent. The difference in the exponents, however, becomes noticeable only in the limit of extremely large molecular weights. In the currently accessible experimental range of $N_B \lesssim 10^3$, the difference can hardly be detected, but we did observe a reasonably wide region of crew-cut spherical micelles (see Figure 8).

In crew-cut micelles of all considered morphologies the equilibrium structure is largely determined by the balance of the free energy of the corona and the surface energy of the core. Since the crew-cut corona is almost planar, its free energy is weakly dependent on the morphology type. The free energy per chain of the spherical corona is slightly smaller than that of cylindrical corona, which in turn is smaller than the free energy per chain of the lamellar corona. Therefore, the free energy of the corona increases upon transition from spheres to cylinders and from cylinders to lamellar. However, this small increase is balanced by the decrease of the elastic free energy of the core. Here we emphasize that the equilibrium surface area per molecule s_j is almost the same for spheres, cylinders, and lamellae. Therefore, micelles of different morphologies demonstrate a similar corona thickness, whereas the core radius varies with micelle morphology as $R_j \approx jR_1$ which is the direct consequence of eq 3.

One of the major goals of this paper was to compare the predictions of the theoretical model with a well-defined set of polystyrene–polyisoprene (PS–PI) diblock copolymers in the selective solvent heptane. To facilitate the comparison between the theory and experiment, we first adjusted the model parameters. This adjustment was done on the basis of data for spherical micelles that were found at larger molecular weights of polyisoprene (corona) block A . The adjusted set of model parameters allowed us to consider self-consistently both the spherical and the cylindrical micelles and to properly describe the sphere-to-cylinder transition. We note that our choice of model parameters was not the only possible one due to the uncertainty in the available experimental data. Moreover, the fit to experimental data for spherical micelles was equally good when certain model parameters deviated by 10–20% from the chosen values. We plan to specify the set of model parameters more precisely when new experiments will be done.

In our studies we observe precipitation of the micelles near the calculated cylinder to lamella transition. On the basis of the prediction of ref 7 and our calculations, we believe that the observed precipitation is due to the cylinder-to-lamella morphological transition. However, at this time we do not have any direct experimental evidence to prove that the micelles adopt a lamellar morphology. We delineated the degree of polymerization

N_A^{cl} of the corona block A corresponding to phase separation of the solution, $N_A^{cl} \sim N_B^{8/11}$. When $N_A > N_A^{cl}$, the solution with giant cylindrical micelles is stable. However, when $N_A < N_A^{cl}$, the cylindrical micelles transform into bilayers that precipitate from the solution. In a good solvent, $N_A^{cl} \sim N_B^{2/3}$. The same scaling dependence, $N_A^{cl} \sim N_B^{2/3}$, for block copolymer precipitation was obtained in ref 7 by using a different argument. Precipitation of the block copolymer solution allows us to determine the value of N_A^{cl} rather precisely and to evaluate the respective stability range $\Delta N_A/N_A^{cl}$ of the cylindrical micelles. We found a good agreement between the experimental value $\Delta N_A/N_A^{cl} = 0.37$ determined for PS-PI block copolymers with $N_B = 393$ and the theoretical values $\Delta N_A/N_A^{cl} = 0.50$ (numerical solution) and $\Delta N_A/N_A^{cl} = 0.31$ (asymptotic solution, eq AIII.10). For good solvent for block A , the asymptotic width of the cylinder region is $\Delta N_A/N_A^{cl} = 0.28$ (eq AIII.10). Note that the asymptotic width determined along the insoluble block axis is independent of solvent quality for the soluble block $\Delta N_B/N_B^{cl} = 0.31$ (eq. AIII.7). Experiments on block copolymer with different molecular weights of polystyrene (core) block would allow further testing of the theoretical diagram of states.

In conclusion, we performed a theoretical investigation of dilute solution of neutral diblock copolymer micelles in selective solvent. We demonstrated that all transitions between different micellar morphologies occur in or near the crew-cut regime. We found a good agreement between theoretically predicted and experimentally measured regions of stability of micelles of different morphologies as well as the sizes and aggregation numbers of micelles. However, many aspects of the problem were not addressed in this study (finite length of the cylindrical and lamellar aggregates, possible polydispersity of block copolymer, etc.). We plan to address these issues in forthcoming publications.

Note Added in Proof. While the paper was in production we learned that Lodge et al. have observed transitions between spheres, cylinders, and vesicles by varying the solvent composition for PS-b-PI diblocks.³⁷

Acknowledgment. E.B.Z. acknowledges the financial support from the STC Program of the National Science Foundation under Agreement CHE-9876674 as well as from Russian Fund for Fundamental Research (RFBR 02-0333127). M.R. acknowledges the support from NSF Grants ECS-0103307 and CHE-9876674 and of the NASA URETI on Bioinspired Materials award NCC-1-02037. We thank D. Lairez (LLB, Saclay France) and M. Rawiso (ICS Strasbourg, France) for having performed the SANS and SAXS measurement of the core radius of the elongated micelles. We also thank NIST for providing SANS facilities for measurements of the core of spherical micelles under the agreement #S15-14.

Appendix I. Polymer Brushes

The structure of polymer brushes in solvents of various quality was considered in a number of previous studies.^{20,22,26} Effective monomer–monomer interactions in good solvents are governed by the excluded-volume parameter $\nu > 0$. In a Θ solvent, the ternary interactions with three-body interaction parameter $w > 0$ are dominant. Below we introduce the solvent-dependent

coefficients that include the excluded-volume and three-body interaction parameters, ν and w , stiffness parameter p_A , and numerical prefactors C_H and C_F

$$\hat{C}_H = \begin{cases} C_H p_A^{1/3} \nu^{1/3} & \nu = 3/5 \\ C_H p_A^{1/4} w^{1/4} & \nu = 1/2 \end{cases} \quad (\text{AI.1})$$

and

$$\hat{C}_F = \begin{cases} C_F & \nu = 3/5 \\ C_F p_A^{-3/4} w^{1/4} & \nu = 1/2 \end{cases} \quad (\text{AI.2})$$

Introduction of the solvent-dependent coefficients \hat{C}_H and \hat{C}_F allows one to express free energy F_j and thickness H_j in the brush of morphology j in terms of degree of polymerization N_A , area per chain s , and scaling exponent ν . In a Θ solvent ($\nu = 1/2$), three-body interaction parameter w can be incorporated into numerical prefactors C_H and C_F . This is equivalent to assigning $w = 1$ in eqs AI.1 and AI.2, leading to simplified expressions for a Θ solvent

$$\hat{C}_H = C_H p_A^{1/4} \quad \text{for } \nu = 1/2 \quad (\text{AI.1a})$$

$$\hat{C}_F = C_F p_A^{-3/4} \quad \text{for } \nu = 1/2 \quad (\text{AI.2a})$$

1. Planar Brush ($j = 1$). The correlation blob size, ξ_A , in a planar brush is independent of distance x from the surface. However, the size and the spacial arrangement of correlation blobs depend on the solvent quality and chain flexibility. Grafted chains in a good solvent form a melt of densely packed blobs with size $\xi_A \approx \sqrt{s}$. For stiffer chains (with Kuhn segment larger than monomer size) in a Θ solvent, the correlation blobs form a string of nonoverlapping blobs in the normal direction but overlap laterally ($\xi_A > \sqrt{s}$) (see ref 26 for details). This occurs because the correlation blob size, ξ_A , depends not only on the surface area per chain, s , but also on the stiffness parameter p_A . Therefore, the relation between the polymer concentration, c , and the correlation blob size, ξ_A , should be written as $c \approx g_A s^{-1} \xi_A^{-1}$. Applying eq 12 to express g_A as a function of ξ_A and using the definition of the correlation blob (chain segment with energy of monomer–monomer interactions $kT \approx kT w a^6 g_A c^2$), we find $\xi_A \approx p_A^{3/4} \sqrt{s}$.²⁶ Then the thickness $H_1 \approx \xi_A (N_A/g_A)$ and the free energy per chain $F_{A1} \approx kT (H_1/\xi_A)$ in a planar brush are given respectively by²⁶

$$H_1 = a_A \hat{C}_H N_A (s a_A^{-2})^{(\nu-1)/2\nu} \quad (\text{AI.3})$$

$$F_{A1}/kT = \hat{C}_H \hat{C}_F N_A (s a_A^{-2})^{-1/2\nu} \quad (\text{AI.4})$$

It should be noted that in the Appendices we continue with the same notations for s used in the main part of the paper, where s is the generalized (unrestricted) value of the surface area per chain.

2. Cylindrical Brush ($j = 2$). A cylindrical brush can be obtained by bending a planar brush. This leads to an increase in the area per chain with distance x from the axis of the cylinder

$$s(x) = s \frac{x}{R_2} \quad (\text{AI.5})$$

where R_2 is the radius of the cylindrical core. We assume that the local structure of the cylindrical layer at distance x coincides with that of a planar layer with grafting area $s(x)$ given by eq AI.5. Then the free energy of the cylindrical corona can be calculated using the free energy density of the planar brush by the following procedure. The free energy density in the planar brush with area s per chain and volume sH_1 pervaded by a chain is

$$\psi(s) = \frac{F_{A1}}{sH_1} = \frac{\hat{C}_F}{s^{3/2}} kT \quad (\text{AI.6})$$

The average density of A monomers in a planar brush is

$$c(s) = \frac{N_A}{sH_1} = \hat{C}_H^{-1} a_A^{-3} (s/a_A^2)^{(1-3\nu)/(2\nu)} \quad (\text{AI.7})$$

In a planar brush both free energy density $\psi(s)$ and polymer concentration $c(s)$ do not depend on distance x from the surface. In contrast to a planar brush, both the free energy density ψ and the monomer concentration c in a cylindrical brush depend on distance x through eq AI.5. Correspondingly, the free energy per chain F_{A2} of the cylindrical corona can be calculated by integrating the free energy density over the volume occupied by the A blocks

$$\frac{F_{A2}}{kT} = \int_{R_2}^{R_2+H_2} \frac{\psi(s)}{kT} s(x) dx = \hat{C}_F \int_{R_2}^{R_2+H_2} s(x)^{-1/2} dx \quad (\text{AI.8})$$

where H_2 is the thickness of the cylindrical brush. The condition of conservation of the number of A monomers per block in the corona

$$N_A = \int_{R_2}^{R_2+H_2} c(s) s(x) dx = \hat{C}_H^{-1} a_A^{-1/\nu} \int_{R_2}^{R_2+H_2} s(x)^{(1-\nu)/(2\nu)} dx \quad (\text{AI.9})$$

provides the equation to determine H_2 . By substituting eq AI.5 for area $s(x)$, we find that the thickness of the cylindrical corona H_2 can be related to the thickness H_1 of the planar brush (eq AI.3) with the same surface area s per chain and to the radius R_2 of the cylindrical core as

$$\begin{aligned} H_2 &= R_2 \left[\left(1 + \frac{(1+\nu)H_1}{2\nu R_2} \right)^{2\nu/(1+\nu)} - 1 \right] \\ &= H_1 \frac{R_2}{H_1} \left[\left(1 + \frac{(1+\nu)H_1}{2\nu R_2} \right)^{2\nu/(1+\nu)} - 1 \right] \quad (\text{AI.10}) \end{aligned}$$

whereas the corona free energy per chain F_{A2} yields

$$\begin{aligned} \frac{F_{A2}}{kT} &= \frac{2\hat{C}_F R_2}{\sqrt{s}} \left[\left(1 + \frac{(1+\nu)H_1}{2\nu R_2} \right)^{\nu/(1+\nu)} - 1 \right] \\ &= \frac{F_{A1}}{kT} \frac{2R_2}{H_1} \left[\left(1 + \frac{(1+\nu)H_1}{2\nu R_2} \right)^{\nu/(1+\nu)} - 1 \right] \quad (\text{AI.11}) \end{aligned}$$

Depending on the value of the ratio H_2/R_2 , we distinguish between bottle-brush ($H_2/R_2 \gg 1$) and crew-cut ($H_2/R_2 \ll 1$) coronas of the cylindrical aggregate. Note that bottle-brush corresponds to the ratio H_1/R_2

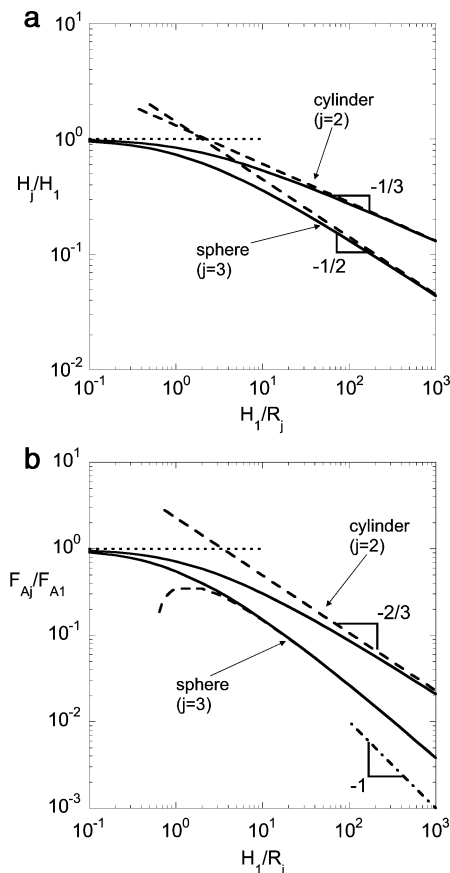


Figure 9. Dependences of a reduced thickness (a) and the reduced free energy (b) of cylindrical (eqs AI.14 and AI.15) and spherical (eqs AI.25 and AI.26) micellar corona as functions of reduced core radius in a Θ solvent for a corona block in double-logarithmic coordinates. Asymptotes are shown by dotted (crew-cut) and dashed (starlike) lines with the exponents indicated in the figure. The dashed-dotted line is the power law asymptote of the free energy of a starlike spherical micelle without logarithmic correction.

$\gg 1$, while crew-cut with $H_2 \approx H_1$, corresponds to $H_1/R_2 \ll 1$. Figure 9 demonstrates reduced corona thickness H_2/H_1 and reduced corona free energy F_{A2}/F_{A1} as a function of reduced curvature H_1/R_2 for a Θ solvent for A block (figure for good solvent looks qualitatively similar). For a bottle-brush corona with thickness H_2 much larger than core radius R_2 , $H_2/R_2 \gg 1$, retention of the leading terms in eqs AI.10 and AI.11 gives asymptotic scaling laws^{26,27}

$$H_2 = R_2^{(1-\nu)/(1+\nu)} \left(\frac{(1+\nu)H_1}{2\nu} \right)^{2\nu/(1+\nu)} \sim \left(\frac{R_2}{s} \right)^{(1-\nu)/(1+\nu)} N_A^{2\nu/(1+\nu)} \quad (\text{AI.12})$$

$$\frac{F_{A2}}{kT} = \frac{2\hat{C}_F R_2}{\sqrt{s}} \left(\frac{(1+\nu)H_1}{2\nu} \right)^{\nu/(1+\nu)} \sim \left(\frac{R_2}{s} \right)^{1/(1+\nu)} N_A^{\nu/(1+\nu)} \quad (\text{AI.13})$$

These asymptotic dependences (eqs AI.12 and AI.13) can be also presented as

$$\frac{H_2}{H_1} = \left(\frac{1+\nu}{2\nu} \right)^{2\nu/(1+\nu)} \left(\frac{R_2}{H_1} \right)^{(1-\nu)/(1+\nu)} \quad (\text{AI.14})$$

$$\frac{F_{A2}}{F_{A1}} = 2 \left(\frac{1+\nu}{2\nu} \right)^{\nu/(1+\nu)} \left(\frac{R_2}{H_1} \right)^{1/(1+\nu)} \quad (\text{AI.15})$$

which are shown by dashed lines in Figure 9 (for $\nu = 1/2$). Asymptotic dependences for bottle-brush micelles are good approximations only for very long coronas, $H_2 > 100R_2$. However, we will see that copolymers with this large block asymmetry prefer to associate into spherical micelles. Cylindrical micelles are relevant for $H_2 < R_2$.

For a crew-cut corona with $H_2/R_2 \ll 1$, expansion of eqs AI.10 and AI.11 with respect to small parameter H_1/R_2 gives

$$H_2 = H_1 \left(1 - \frac{1-\nu}{4\nu} \frac{H_1}{R_2} + \dots \right) \quad (\text{AI.16})$$

$$\frac{F_{A2}}{kT} = \frac{\hat{C}_F H_1}{\sqrt{s}} \left(1 - \frac{1}{4\nu} \frac{H_1}{R_2} + \dots \right) = \frac{F_{A1}}{kT} \left(1 - \frac{1}{4\nu} \frac{H_1}{R_2} + \dots \right) \quad (\text{AI.17})$$

where H_1 and F_{A1} are given by eqs AI.3 and AI.4, respectively. Therefore, the free energy of a crew-cut cylindrical corona can be presented as the free energy of a planar brush minus corrections due to the curvature. The dominant (first) terms in these asymptotes (planar brush) are indicated by the horizontal dotted lines in Figure 9. In asymptotic expressions in section 3 we retain only the leading corrections to the planar brush expressions (second terms in brackets on the right-hand side in eqs AI.16 and AI.17) due to the curvature of the core.

Free energy F_{A2} and thickness H_2 of the cylindrical corona can be written in terms of dimensionless radius of the cylinder $r_2 = R_2/a_B$ using eqs 4, AI.3, AI.10, and AI.11

$$\frac{F_{A2}}{kT} = 2\hat{C}_F r_2^{3/2} \left(\frac{\varphi}{2N_B} \right)^{1/2} \left\{ \left[1 + \frac{1+\nu}{2\nu} \left(\frac{a_A}{a_B} \right)^{1/\nu} \hat{C}_H N_A r_2^{(1-3\nu)/(2\nu)} \left(\frac{2N_B}{\varphi} \right)^{(\nu-1)/(2\nu)} \right]^{\nu/(1+\nu)} - 1 \right\} \quad (\text{AI.18})$$

$$H_2 = R_2 \left\{ \left[1 + \frac{1+\nu}{2\nu} \left(\frac{a_A}{a_B} \right)^{1/\nu} \hat{C}_H N_A r_2^{(1-3\nu)/(2\nu)} \left(\frac{2N_B}{\varphi} \right)^{(\nu-1)/(2\nu)} \right]^{2\nu/(1+\nu)} - 1 \right\} \quad (\text{AI.19})$$

3. Spherical Brush ($j = 3$). In a spherical corona the area per chain depends on distance x from the center of the micelle as

$$s(r) = s \left(\frac{x}{R_3} \right)^2 \quad (\text{AI.20})$$

By performing the same calculation as for a cylindrical brush (i.e., by substituting expression AI.20 into eqs AI.8 and AI.9 and replacing $j = 2$ by $j = 3$), we find that the thickness H_3 of the spherical corona is given by

$$H_3 = R_3 \left[\left(1 + \frac{H_1}{\nu R_3} \right)^\nu - 1 \right] = H_1 \frac{R_3}{H_1} \left[\left(1 + \frac{H_1}{\nu R_3} \right)^\nu - 1 \right] \quad (\text{AI.21})$$

whereas the free energy per chain F_{A3} yields

$$\frac{F_{A3}}{kT} = \frac{\nu \hat{C}_F R_3}{\sqrt{s}} \ln \left(1 + \frac{H_1}{\nu R_3} \right) = \frac{F_{A1}}{kT} \frac{\nu R_3}{H_1} \ln \left(1 + \frac{H_1}{\nu R_3} \right) \quad (\text{AI.22})$$

Here, $R_3 = 3N_B a_B^3 (\varphi s)^{-1}$ is the radius of the spherical core (see eq 3). Reduced thickness H_3/H_1 and reduced free energy F_{A3}/F_{A1} are plotted as solid lines in Figure 9a,b as functions of reduced curvature H_1/R_3 for the case of a Θ solvent.

In the limit of starlike corona ($H_3/R_3 \gg 1$ or, equivalently, $H_1/R_3 \gg 1$), the thickness H_3 and the free energy F_{A3} are obtained from eqs AI.21 and AI.22 to give^{25,26}

$$H_3 = R_3^{(1-\nu)} \left(\frac{H_1}{\nu} \right)^\nu \sim \left(\frac{R_3^2}{s} \right)^{(1-\nu)/2} N_A^\nu \quad (\text{AI.23})$$

$$\frac{F_{A3}}{kT} = \frac{\nu \hat{C}_F R_3}{\sqrt{s}} \ln \left(\frac{H_1}{\nu R_3} \right) \sim \left(\frac{R_3^2}{s} \right)^{1/2} \quad (\text{AI.24})$$

These asymptotic dependences can be also presented as

$$\frac{H_3}{H_1} = \left(\frac{1}{\nu} \right)^\nu \left(\frac{R_3}{H_1} \right)^{1-\nu} \quad (\text{AI.25})$$

$$\frac{F_{A3}}{F_{A1}} = \nu \frac{R_3}{H_1} \ln \left(\frac{H_1}{\nu R_3} \right) \quad (\text{AI.26})$$

(dashed lines in Figure 9a,b for $\nu = 1/2$). The dash-dotted line in Figure 9b with the slope -1 corresponds to the leading power law term in the free energy of starlike corona asymptote ($F_{A3}/F_{A1} = \nu R_3/H_1$). This simple power law scaling significantly underestimates the free energy of starlike micelles, making logarithmic correction very important for accurate calculations.

For crew-cut corona ($H_3/R_3 \ll 1$ or, equivalently, $H_1/R_3 \ll 1$)

$$H_3 = H_1 \left(1 - \frac{1-\nu}{2\nu} \frac{H_1}{R_3} + \dots \right) \quad (\text{AI.27})$$

$$\frac{F_{A3}}{kT} = \frac{F_{A1}}{kT} \left(1 - \frac{1}{2\nu} \frac{H_1}{R_3} + \dots \right) \quad (\text{AI.28})$$

Similarly to the case of cylindrical crew-cut coronas, the free energy of spherical crew-cut coronas includes negative corrections due to the curvature. We retain below only the leading corrections (second terms in eqs AI.27 and AI.28) to the thickness H_1 and the free energy F_{A1} of the planar brush. Note that curvilinear corrections to the corona thickness and free energy of spherical micelles are twice larger than corrections for cylindrical micelles.

Free energy F_{A3} and thickness H_3 of the spherical corona can be expressed in terms of dimensionless radius of the sphere $r_3 = R_3/a_B$ using eqs 4, AI.3, AI.21, and AI.22

$$\frac{F_{A3}}{kT} = \nu \hat{C}_F r_3^{3/2} \left(\frac{\varphi}{3N_B} \right)^{1/2} \ln \left[1 + \frac{1}{\nu} \left(\frac{a_A}{a_B} \right)^{1/\nu} \hat{C}_H N_A r_3^{(1-3\nu)/(2\nu)} \left(\frac{3N_B}{\varphi} \right)^{(\nu-1)/(2\nu)} \right] \quad (\text{AI.29})$$

$$H_3 = R_3 \left\{ \left[1 + \frac{1}{\nu} \left(\frac{a_A}{a_B} \right)^{1/\nu} \hat{C}_H N_A r_{3star}^{(1-3\nu)/(2\nu)} \left(\frac{3N_B}{\varphi} \right)^{(\nu-1)/(2\nu)} \right]^\nu - 1 \right\} \quad (\text{AI.30})$$

Appendix II. Polymer Micelles

1. Starlike Spherical Micelle, $H_3 \gg R_3$. In a starlike spherical micelle, the corona free energy per chain yields

$$F_{A3star}/kT \approx \nu \hat{C}_F r_{3star}^{3/2} \left(\frac{\varphi}{3N_B} \right)^{1/2} \ln \left[\frac{1}{\nu} \left(\frac{a_A}{a_B} \right)^{1/\nu} \hat{C}_H N_A r_{3star}^{(1-3\nu)/(2\nu)} \left(\frac{3N_B}{\varphi} \right)^{(\nu-1)/(2\nu)} \right] \quad (\text{AII.1})$$

This expression is obtained by neglecting unity in the argument of the logarithm in eq AI.29. The surface free energy can be written using eq 4

$$F_{s3}/kT = \gamma s a_B^{-2} = \frac{3\gamma N_B}{\varphi r_{3star}}$$

By minimizing ($F_{A3star} + F_{s3}$) with respect to dimensionless radius of the core $r_{3star} = R_{3star}/a_B$, we find

$$r_{3star} = \left(\frac{2\gamma}{3\nu K \hat{C}_F} \right)^{2/5} \left(\frac{3N_B}{\varphi} \right)^{3/5} \quad (\text{AII.2})$$

where the logarithm is defined by

$$K = \ln \left[\frac{1}{\nu} \left(\frac{a_A}{a_B} \right)^{1/\nu} \hat{C}_H N_A r_{3star0}^{(1-3\nu)/(2\nu)} \left(\frac{3N_B}{\varphi} \right)^{(\nu-1)/(2\nu)} \right] \quad (\text{AII.3})$$

and the core size without the logarithmic correction is given by

$$r_{3star0} = \left(\frac{2\gamma}{3\nu \hat{C}_F} \right)^{2/5} \left(\frac{3N_B}{\varphi} \right)^{3/5} \quad (\text{AII.4})$$

Thickness of the corona H_{3star} in a starlike micelle is obtained by retaining the dominant term in eq AI.30

$$H_{3star} = a_A N_A \nu \left(\frac{\hat{C}_H}{\nu} \right)^\nu \left(\frac{2\gamma}{3\nu K \hat{C}_F} \right)^{3(1-\nu)/5} \left(\frac{3N_B}{\varphi} \right)^{2(1-\nu)/5} \quad (\text{AII.5})$$

whereas aggregation number Q_{3star} is given by

$$Q_{3star} = 4\pi \left(\frac{2\gamma}{3\nu K \hat{C}_F} \right)^{6/5} \left(\frac{3N_B}{\varphi} \right)^{4/5} \quad (\text{AII.6})$$

Equilibrium free energy yields

$$\frac{F_{3star}}{kT} = \frac{5}{3} \gamma^{3/5} \left(\frac{9\nu \hat{C}_F N_B K}{2\varphi} \right)^{2/5} \quad (\text{AII.7})$$

2. Crew-Cut Micelles, $H_j \ll R_j$. In a crew-cut micelle, a convenient variable to express the free energy is the area s per chain. Here, the corona is almost planar and the dominant contribution to its free energy is given by eq AI.4. Correspondingly, the equilibrium parameters of crew-cut micelles of all the morphologies obey the same scaling dependences. The free energy per chain in a crew-cut micelle with area per chain s yields

$$F_{jcc}/kT \approx \gamma s a_B^{-2} + \hat{C}_H \hat{C}_F N_A (s a_A^{-2})^{-1/(2\nu)} \quad (\text{AII.8})$$

By minimizing F_{jcc} with respect to s , we find

$$\frac{s_{cc}}{a_B^2} = \left[\frac{N_A}{2\nu\gamma} \hat{C}_H \hat{C}_F \left(\frac{a_A}{a_B} \right)^{1/\nu} \right]^{2\nu/(1+2\nu)} \quad (\text{AII.9})$$

Free energy of the corona $F_{Ajcc} \approx F_{A1cc}$ is given by substituting eq AII.9 into eq AI.4

$$\frac{F_{A1cc}}{kT} = 2\nu\gamma^{1/(1+2\nu)} \left[\frac{N_A}{2\nu} \hat{C}_H \hat{C}_F \left(\frac{a_A}{a_B} \right)^{1/\nu} \right]^{2\nu/(1+2\nu)} \quad (\text{AII.10})$$

whereas the leading (corona and surface) part of the free energy per chain is approximately the same as in the planar case $F_{jcc} \approx F_{1cc}$ (using eqs AII.8 and AII.9) and can be written as

$$\frac{F_{1cc}}{kT} = (1 + 2\nu)\gamma^{1/(1+2\nu)} \left[\frac{N_A}{2\nu} \hat{C}_H \hat{C}_F \left(\frac{a_A}{a_B} \right)^{1/\nu} \right]^{2\nu/(1+2\nu)} \quad (\text{AII.11})$$

The radius of the core R_{jcc} in a micelle of morphology j ($j = 1, 2, 3$), and corona thickness $H_{jcc} \approx H_{1cc}$ are respectively obtained using eqs 3, AI.3, and AII.9

$$R_{jcc} = a_B \frac{jN_B}{\varphi} \left[\frac{N_A}{2\nu\gamma} \hat{C}_H \hat{C}_F \left(\frac{a_A}{a_B} \right)^{1/\nu} \right]^{-2\nu/(1+2\nu)} \quad (\text{AII.12})$$

$$H_{jcc} = a_A (N_A \hat{C}_H)^{3\nu/(1+2\nu)} \left(\frac{\hat{C}_F}{2\nu\gamma} \right)^{(\nu-1)/(1+2\nu)} \left(\frac{a_A}{a_B} \right)^{2(1-\nu)/(1+2\nu)} \quad (\text{AII.13})$$

Aggregation number in a spherical ($j = 3$) crew-cut micelle is calculated using eqs 4, 17, AII.9, and AII.12

$$Q_{3cc} = \frac{4\pi R_{3cc}^2}{s_{cc}} = \frac{36\pi N_B^2}{\varphi^2} \left[\frac{N_A}{2\nu\gamma} \hat{C}_H \hat{C}_F \left(\frac{a_A}{a_B} \right)^{1/\nu} \right]^{-6\nu/(1+2\nu)} \quad (\text{AII.14})$$

The linear density of block copolymer molecules in a cylindrical crew-cut micelle ρ_{cc} (number of chains per unit length of the cylinder) is derived using eqs 34 and AII.12

$$\rho_{cc} = \frac{\pi r_{2cc}^2 \varphi}{a_B N_B} = \frac{4\pi N_B}{a_B \varphi} \left[\frac{N_A}{2\nu\gamma} \hat{C}_H \hat{C}_F \left(\frac{a_A}{a_B} \right)^{1/\nu} \right]^{-4\nu/(1+2\nu)} \quad (\text{AII.15})$$

whereas the surface density of chains in a crew-cut lamella is $1/s_{cc}$.

3. Bottle-Brush Cylindrical Micelle. In a bottle-brush cylindrical micelle, corona free energy is obtained by retaining the dominant contribution in eq AI.18

$$\frac{F_{A2bb}}{kT} = 2\hat{C}_F \left(\frac{1 + \nu \hat{C}_H N_A}{2\nu} \right)^{\nu(1+\nu)} \left(\frac{a_A}{a_B} \frac{\varphi}{2N_B} r_{2bb}^2 \right)^{1/(1+\nu)} \quad (\text{AII.16})$$

whereas surface free energy (eq 8) yields

$$F_{s2}/kT = \gamma s a_B^{-2} = \frac{2\gamma N_B}{\varphi r_2} \quad (\text{AII.17})$$

By minimizing ($F_{A2bb} + F_{s2}$) with respect to dimension-

less radius of the cylinder $r_2 = R_2/a_B$, we find

$$r_{2bb} = \left(\frac{1 + \nu}{4} \frac{a_B}{a_A} \right)^{1/(3+\nu)} \left(\frac{2N_B}{\varphi} \right)^{(2+\nu)/(3+\nu)} \left(\frac{\gamma}{\hat{C}_F} \right)^{(1+\nu)/(3+\nu)} \left(\frac{2\hat{C}_H N_A}{\nu} \right)^{-\nu/(3+\nu)} \quad (\text{AII.18})$$

The corresponding free energy per chain in a bottle-brush cylindrical micelle is

$$\frac{F_{2bb}}{kT} \approx \left(\frac{a_A}{a_B} \frac{N_B}{\varphi} \right)^{1/(3+\nu)} \gamma^{2/(3+\nu)} \hat{C}_F^{(1+\nu)/(3+\nu)} \hat{C}_H^{\nu/(3+\nu)} N_A^{\nu/(3+\nu)} \quad (\text{AII.19})$$

Appendix III. Morphological Transitions

Morphological transitions sphere–cylinder–lamella occur when micelles have the crew-cut shape. In a micelle of morphology j the corona free energy can be represented as

$$F_{Ajcc} \approx F_{A1cc} \left[1 - \frac{(j-1)}{4\nu} \frac{H_1(s_{cc})}{R_{jcc}(s_{cc})} \right] \quad (\text{AIII.1})$$

where free energy F_{A1cc} of the crew-cut corona and area per chain s_{cc} are given by eqs AII.10 and AII.9, whereas core radius R_{jcc} and corona thickness H_{jcc} are respectively given by eqs AII.12 and AI.13. The total free energy per chain $F_j = F_{Ajcc} + F_{sj} + F_{Bj}$ yields

$$\frac{F_j}{kT} \approx \frac{F_{1cc}(s_{cc})}{kT} - F_{A1cc}(s_{cc}) \frac{(j-1)}{4\nu j} \frac{H_{1cc}(s_{cc}) s_{cc} \varphi}{N_B a_B^3} + k_j \frac{j^2 N_B (a_B^2)^2}{p_B \varphi^2 (s_{cc})^2} \quad (\text{AIII.2})$$

where k_j are the numerical coefficients given by eq 7 and $F_{1cc}(s_{cc})$ is the leading (corona and surface) part of the free energy of lamella. The second and third terms in eq AIII.2 are corrections to corona and core due to curvature. By substituting s_{cc} from eq AII.9 into eq AIII.2, we find

$$\frac{F_j}{kT} \approx \frac{F_{1cc}(s_{cc})}{kT} - \frac{(j-1)}{2j} \gamma^{(2-3\nu)/(1+2\nu)} \left[N_A \hat{C}_H \left(\frac{a_A}{a_B} \right)^{1/\nu} \right]^{7\nu/(1+2\nu)} \left(\frac{\hat{C}_F}{2\nu} \right)^{(5\nu-1)/(1+2\nu)} \frac{\varphi}{N_B} + k_j \frac{j^2 N_B}{\varphi^2 p_B} \left[\frac{N_A \hat{C}_H \hat{C}_F (a_A)^{1/\nu}}{2\nu \gamma} \right]^{-4\nu/(1+2\nu)} \quad (\text{AIII.3})$$

The morphological transition $(j+1) \Rightarrow j$ is specified by the condition $F_{j+1} = F_j$ to give the following equation for the binodals

$$N_B^2 = \frac{\varphi^3 p_B \gamma^{(2-7\nu)/(1+2\nu)}}{2j(j+1)[k_{j+1}(j+1)^2 - k_j j^2]} \left[N_A \hat{C}_H \left(\frac{a_A}{a_B} \right)^{1/\nu} \right]^{11\nu/(1+2\nu)} \left(\frac{\hat{C}_F}{2\nu} \right)^{(9\nu-1)/(1+2\nu)} \quad (\text{AIII.4})$$

By substituting $j = 2$ in eq AIII.4 and solving it with respect to N_B , we find the asymptotic expression for the binodal $N_B^{\text{sc}} = N_B^{\text{sc}}(N_A)$, corresponding to sphere-to-cylinder transition

$$N_B^{\text{sc}} = \frac{2}{\pi} \sqrt{\frac{5}{21}} \varphi^{3/2} p_B^{1/2} \gamma^{(2-7\nu)/[2(1+2\nu)]} \left[N_A \hat{C}_H \left(\frac{a_A}{a_B} \right)^{1/\nu} \right]^{11\nu/[2(1+2\nu)]} \left(\frac{\hat{C}_F}{2\nu} \right)^{(9\nu-1)/[2(1+2\nu)]} \quad (\text{AIII.5})$$

By substituting $j = 1$ in eq AIII.4, we find the asymptotic expression for the binodal $N_B^{\text{cl}} = N_B^{\text{cl}}(N_A)$, corresponding to cylinder-to-lamella transition

$$N_B^{\text{cl}} = \frac{\sqrt{2}}{\pi} \varphi^{3/2} p_B^{1/2} \gamma^{(2-7\nu)/[2(1+2\nu)]} \left[N_A \hat{C}_H \left(\frac{a_A}{a_B} \right)^{1/\nu} \right]^{11\nu/[2(1+2\nu)]} \left(\frac{\hat{C}_F}{2\nu} \right)^{(9\nu-1)/[2(1+2\nu)]} \quad (\text{AIII.6})$$

The asymptotic value of the relative width of the stability region for cylindrical micelle

$$\frac{\Delta N_B}{N_B^{\text{cl}}} = \frac{N_B^{\text{cl}} - N_B^{\text{sc}}}{N_B^{\text{cl}}} = 1 - \sqrt{\frac{10}{21}} \approx 0.31 \quad (\text{AIII.7})$$

is therefore independent of the solvent strength (the value of ν). By inverting eqs AIII.5 and AIII.6, we find the asymptotic expressions of the binodals $N_A^{\text{sc}} = N_A^{\text{sc}}(N_B)$ and $N_A^{\text{cl}} = N_A^{\text{cl}}(N_B)$, corresponding to sphere-to-cylinder and cylinder-to-lamella transitions

$$N_A^{\text{sc}} = \left(\frac{21\pi^2}{20} \frac{N_B^2}{p_B \varphi^3} \right)^{(1+2\nu)/(11\nu)} \gamma^{(7\nu-2)/(11\nu)} \left(\frac{a_B}{a_A} \right)^{1/\nu} \left(\frac{\hat{C}_F}{2\nu} \right)^{(1-9\nu)/(11\nu)} \quad (\text{AIII.8})$$

$$N_A^{\text{cl}} = \left(\frac{\pi^2}{2} \frac{N_B^2}{p_B \varphi^3} \right)^{(1+2\nu)/(11\nu)} \gamma^{(7\nu-2)/(11\nu)} \left(\frac{a_B}{a_A} \right)^{1/\nu} \left(\frac{\hat{C}_F}{2\nu} \right)^{(1-9\nu)/(11\nu)} \quad (\text{AIII.9})$$

where \hat{C}_H and \hat{C}_F are given by eqs AI.1 and AI.2. The asymptotic value of the relative width of the stability region for cylindrical micelle in these variables depends on the value of ν as

$$\frac{\Delta N_A}{N_A^{\text{cl}}} = \frac{N_A^{\text{sc}} - N_A^{\text{cl}}}{N_A^{\text{cl}}} = \left(\frac{21}{10} \right)^{(1+2\nu)/(11\nu)} - 1 \approx \begin{cases} 0.28 & \nu = 3/5 \\ 0.31 & \nu = 1/2 \end{cases} \quad (\text{AIII.10})$$

Table of Notations

A	notation for soluble block
A	Hamaker constant
a_A	size of the soluble monomer
a_B	size of the insoluble monomer
B	notation for insoluble block
C	notation for cylinder
C_F	numerical coefficient (eq AI.2)
\hat{C}_F	solvent-dependent coefficients that includes ν , w , p_a , and C_F
C_H	numerical coefficient (eq AI.1)
\hat{C}_H	solvent-dependent coefficients that includes ν , w , p_a , and C_H
$c(s)$	average density of A monomers (eq AI.7)
C_∞	characteristic ration
C_ξ	numerical coefficient on the order of unity (eq 61)

F_{Aj}	free energy of the micellar corona with morphology j	R_G	Gaussian end-to-end distance (eq 5)
F_{Bj}	free energy of the micellar core with morphology j (eq 6)	R_h	hydrodynamic radius
F_j	total free energy of micelle with morphology j (eq 1)	R_j	radius of core with morphology j (eq 3)
F_{sj}	free energy of the micelle surface with morphology j (eq 8)	r_j	dimensionless core radius with morphology j : $r_j = R_j/a_B$
F_W	van der Waals attraction energy	R_j^{tot}	total size of a micelle with morphology j : $R_j^{\text{tot}} = H_j + R_j$
$F_{1(\text{curv})}$	free energy per chain in curved crew-cut lamella	R_{jcc}	core size of crew-cut micelle with morphology j ($j = 1$, eq 42; $j = 2$, eq 36; $j = 3$, eq 25)
$F_{1(\text{m})}$	free energy per chain in the lamellar mesophase in sediment	$R_{3\text{star}}$	core radius of starlike spherical micelle (eq 18)
F_{2bb}	free energy per chain of bottle-brush cylindrical micelle (eq 35)	$r_{3\text{star}0}$	dimensionless core radius of starlike spherical micelles when $K = 1$ (eq 20)
F_{3cc}	free energy per chain in crew-cut spherical micelle (eq 28)	S	notation for sphere
$F_{3\text{star}}$	free energy per chain of starlike spherical micelle (eq 23)	s	generalized value of the surface area per chain (eq 4)
g_A	number of A monomers inside correlation blob	s_{cc}	area per chain in crew-cut micelle (eq 26)
H_j	corona thickness of micelle with morphology j ($j = 1$, eq 40; $j = 2$, eq 32; $j = 3$, eq 15)	s_j	equilibrium surface area per chain in a micelle with morphology j
$H_{3\text{star}}$	corona thickness in starlike spherical micelle (eq 21)	T	absolute temperature
j	morphology index label (1 = lamella, 2 = cylinder, 3 = sphere, 0 = unimer)	V_0	monomer volume
K	logarithmic term (eq 19)	v	excluded-volume parameter
k	Boltzmann constant	w	three-body interaction parameter
k_j	numerical coefficients: $k_1 = \pi^2/8$, $k_2 = \pi^2/16$, $k_3 = 3\pi^2/80$ (eq 7)	γ	surface free energy per area a_B^2 : $\gamma = \tilde{\gamma}a_B^2$
L	notation for lamellae	$\tilde{\gamma}$	surface free energy per unit area (surface tension)
L	average contour length of cylindrical micelles	Θ	theta temperature
l_A	Kuhn segment size of soluble block	μ_g	chemical potential of globule in dilute phase
l_B	Kuhn segment size of insoluble block	μ_p	chemical potential of polymer in sediment
M	molar mass of polymer	ν	scaling exponent
M_0	molar mass of monomer	ξ_A	correlation blob size of block A (eq 12)
N_A	degree of polymerization of the soluble block	ξ_{last}	last blob in spherical starlike micelle (eq 55)
N_A^{cl}	value of N_A where $F_2 = F_1$ for a set value of N_B (eq AIII.9)	ξ_t	thermal blob size: $\xi_t \approx p_A^2 v^{-1} a_A$
N_A^{sc}	value of N_A where $F_3 = F_2$ for a set value of N_B (eq AIII.8)	ρ	linear density of block copolymer molecules in cylindrical micelle
N_A^0	for $N_A \gg N_A^0$ micelles have crew-cut structure at transitions (eq 49)	ρ_{bulk}	polymer bulk density
N_{Av}	Avogadro's number	ρ_{cc}	linear density of block copolymer molecules in crew-cut cylindrical micelle (eq AII.15)
N_B	degree of polymerization of the insoluble block	σ_1	surface density of chains in lamella
N_B^{**}	degree of polymerization of the B block for a given value of N_A when F_{A3} , F_{B3} , and F_{s3} become the same order of magnitude (eq 29)	τ	relative deviation from theta temperature: $\tau = (T - \Theta)/T$
$N_B^*(N_A)$	degree of polymerization of B block at which the size of the core is equal to the size of the corona for a given value of N_A (eq 24)	φ	volume fraction of B monomers in the micelle core
p_A	stiffness parameter of the soluble block: $p_A = l_A/a_A$	φ'	equilibrium volume fraction of monomers in a dilute phase of phase-separated solutions
PAA	poly(acrylic acid)	ψ	free energy density in planar brush (eq AI.6)
p_B	stiffness parameter of the insoluble block: $p_B = l_B/a_B$		
PB	polybutadiene		
PEO	poly(ethylene oxide)		
PI	polyisoprene		
PS	polystyrene		
Q	aggregation number (total number of chains per micelle) (eq 17)		
Q_{cc}	aggregation number in crew-cut micelle (eq 27)		
$Q_{3\text{star}}$	aggregation number of starlike spherical micelle (eq 22)		
R_{B0}	radius of the core for a single collapsed block B (eq 9)		

References and Notes

- (1) de Gennes, P. G. *Scaling Concepts in Polymer Physics*; Cornell University Press: Ithaca, NY, 1979.
- (2) Rubinstein, M.; Colby, R. H. *Polymer Physics*; Oxford University Press: Oxford, UK, 2003.
- (3) Noolandi, J.; Hong, K. M. *Macromolecules* **1983**, *16*, 1443.
- (4) Zhulina, E. B.; Birshtein, T. M. *Polym. Sci. USSR* **1985**, *27*, 570. Birshtein, T. M.; Zhulina, E. B. *Polymer* **1989**, *30*, 170.
- (5) Halperin, A. *Macromolecules* **1987**, *20*, 2943.
- (6) Izzo, D.; Marques, C. M. *Macromolecules* **1993**, *26*, 7189.
- (7) Izzo, D.; Marques, C. M. *Macromolecules* **1997**, *30*, 6544.
- (8) Hamley, I. W. *The Physics of Block Copolymers*; Oxford University Press: New York, 1998.
- (9) Zhang, L.; Barlow, R. J.; Eisenberg, A. *Macromolecules* **1995**, *28*, 6055.
- (10) Won, Y. Y.; Davis, H. T.; Bates, F. S. *Science* **1999**, *283*, 960.
- (11) Zhang, L.; Eisenberg, A. *Science* **1995**, *268*, 1728.
- (12) Price, C. *Pure Appl. Chem.* **1983**, *55*, 1563.
- (13) Wells, S. L. Ph.D. Thesis, UNC, 2000.
- (14) Larue, I.; Adam, M.; Sheiko, S. S.; Rubinstein, M. *Macromolecules* **2004**, *37*, 5002.
- (15) Larue, I.; Adam, M.; Sheiko, S.; Rubinstein, M. *Polym. Mater. Sci. Eng.* **2003**, *88*, 236.

- (16) Price, C.; Chan, E. K. M.; Hudd, A. L.; Stubbersfield, R. B. *Polym. Commun.* **1986**, *27*, 196.
- (17) Yan, X.; Lui, G.; Li, H. *Langmuir* **2004**, *20*, 4677.
- (18) Won, Y. Y.; Davis, H. T.; Bates, F. S. *Macromolecules* **2003**, *36*, 953.
- (19) Termonia, Y. *J. Polym. Sci.* **2002**, *40*, 890.
- (20) Alexander, S. *J. Phys. (Paris)* **1977**, *38*, 983.
- (21) de Gennes, P. G. *Macromolecules* **1980**, *15*, 235.
- (22) Halperin, A.; Tirrell, M.; Lodge, T. P. *Adv. Polym. Sci.* **1990**, *100*, 31.
- (23) Semenov, A. N. *Sov. Phys. JETP* **1985**, *61*, 733.
- (24) Lairez, D.; Adam, M.; Carton, J. P.; Raspaud, E. *Macromolecules* **1997**, *30*, 6798.
- (25) Daoud, M.; Cotton, J. P. *J. Phys. (Paris)* **1982**, *43*, 531.
- (26) Birshtein, T. M.; Zhulina, E. B. *Polymer* **1984**, *25*, 1453.
- (27) Wang, Z.-G.; Safran, S. A. *J. Chem. Phys.* **1988**, *89*, 5323.
- (28) Safran, A. S. *Statistical Thermodynamics of Surfaces, Interfaces, and Membranes*; Addison-Wesley: Reading, MA, 1994.
- (29) Israelachvili, J. N. *Intermolecular and Surface Forces*; Academic Press: London, 1985.
- (30) We anticipate that van der Waals interaction between undulating cylinders (the attraction energy per persistence length of a cylindrical micelle) is less than kT and therefore is insufficient to cause precipitation of cylindrical aggregates.
- (31) Wang, Z. G. *Macromolecules* **1992**, *25*, 3702.
- (32) Ajdari, A.; Leibler, L. *Macromolecules* **1991**, *24*, 6803.
- (33) Ohta, T.; Nonomura, M. *Eur. Phys. J. B* **1998**, *2*, 57.
- (34) Birshtein, T. M.; Zhulina, E. B. *Macromol. Theory Simul.* **1997**, *6*, 1169.
- (35) Potemkin, I. I. *Eur. Phys. J. E* **2003**, *12*, 207.
- (36) *Physical Properties of Polymers Handbook*; Mark, J. E., Ed.; AIP Press: Woodbury, NY, 1996.
- (37) Lodge, T. P.; Bang, J.; Li, Z.; Hillmyer, M. A.; Talmon, Y. R. *Soc. Chem., Faraday Discuss.* **2005**, *128*, 1.

MA048102N